Corrosion performance of carbon steel in N-doped mesoporous carbon spheres (NMCS)-containing alkaline medium in presence of chloride

Mahmoud, H.

DOI
10.1016/j.mtcomm.2019.100677

Publication date
2019

Document Version
Final published version

Published in
Materials Today Communications

Materials Today Communications 21 (2019) 100677

Contents lists available at ScienceDirect

Materials Today Communications

journal homepage: www.elsevier.com/locate/mtcomm

Corrosion performance of carbon steel in N-doped mesoporous carbon spheres (NMCS)-containing alkaline medium in presence of chloride

H. Mahmoud[a,b,*]

[a] Else Kooi Lab., Faculty of Electrical Engineering, Mathematics and Computer Science, Delft University of Technology, Feldmannweg 17, 2628 CT Delft, the Netherlands
[b] Chemistry Department, Faculty of Science, Zagazig University, Egypt

ARTICLE INFO

Keywords:
Corrosion
N-doped MCSs
Steel passivity
Zeta potential
CV

ABSTRACT

The electrochemical response of carbon steel in chloride-free or chloride-containing 0.1 M and 0.9 M NaOH, in the presence of 0.016 wt.% NMCS, is the subject of this work. The NMCS exhibited a negative (in 0.1 M NaOH) and positive (in 0.9 M NaOH) zeta-potential. This determined altered steel electrochemical response, improved overall, especially in chloride-containing 0.9 M NaOH. The effect was related to an enhanced Fe^{3+} contribution in the passive film, when NMCS were present. The improved corrosion resistance was also attributable to a NMCS-triggered competition of OH^- vs. Cl^- ions in the medium, in other words, NMCS interference to promote passive layer stability.

1. Introduction

Steel corrosion and steel passivation in an alkaline environment, simulating concrete pore water (pH < 12.5), have been extensively studied by different electrochemical techniques [1–11]. The passive film has been described as a bilayer structure (3–15 nm in thickness), consisting of an inner, barrier layer, and an outer one, the latter formed via the hydrolysis of cations ejected from the inner layer [12–14]. It was reported that the inner layer is mainly composed of mixed Fe^{2+} oxides, while the outer layer is relatively richer in Fe^{3+} oxide/hydroxides of a topotactic heterogeneous nature [14,15].

According to the point defect model (PDM) [13,17,18], the passive film is considered as a highly doped, but graded, defect semiconductor structure, in which the vacancies are assumed to act as electronic dopants. An *n*-type semiconducting behavior has been generally accepted for the passive film formed on carbon steel in simulated concrete pore solution [16,18], since the oxygen vacancies or cation interstitials (Fe^{2+}) are the predominant dopants in the passive film [16,18]. On the other hand, the PDM suggests that in the presence of chloride ions, the breakdown of passivity is initiated from a stress fracture in the film, induced by the condensates of cation vacancies (acceptor vacancies) that are generated from the reaction of Cl^- and oxygen vacancies [12,17,19]. Hence, although the structure and composition of the passive film, formed on steel in an alkaline environment, is known and has been widely reported, it is still a controversial subject. This also follows from the variety of well recognized influential factors. For instance, factors such as pH, solution composition, chloride content, additives, etc., can control the steel electrochemical response. These, in turn, affect the semiconducting properties of the passive layer and the overall corrosion response, especially in the case of a chloride-containing environment [7–9,20,21].

Nowadays, carbon-based materials, incorporating allotropes of carbon, e.g. carbon nanotubes (CNTs), carbon nanofibers, and graphene oxide, are being successfully engineered and applied in concrete and reinforced concrete structures. In general, the aim of these additions is to improve the mechanical performance of the bulk matrix, while research on establishing simultaneously enhanced steel corrosion resistance and global performance of the reinforced concrete system is relatively scarce [22–24]. Therefore, achieving a full understanding of the effects of carbon-based additives on the electronic (semi-conductive) properties of the passive film, and consequently, the overall corrosion state of the reinforced concrete structure, is still a challenge.

Among the few available reported studies on the steel electrochemical response in the presence of carbon-based materials [25–31], Sreevatse et al. [31] provided a qualitative investigation of the effect of graphene as an ionic barrier for steel. The authors concluded that the corrosion rate of graphene coated steel was substantially reduced because of the effect of carbon–based materials on the electron donor, *n*-type film on the steel substrate, formed under these conditions [31]. Tong et al. [26] used electrophoretic deposition (EPD) for the

* Corresponding author at: Else Kooi Lab., Faculty of Electrical Engineering, Mathematics and Computer Science, Delft University of Technology, Feldmannweg 17, 2628 CT Delft, the Netherlands.
E-mail address: H.M.AminHassan@tudelft.nl.

https://doi.org/10.1016/j.mtcomm.2019.100677
Received 24 July 2019; Received in revised form 27 September 2019; Accepted 28 September 2019
Available online 02 October 2019

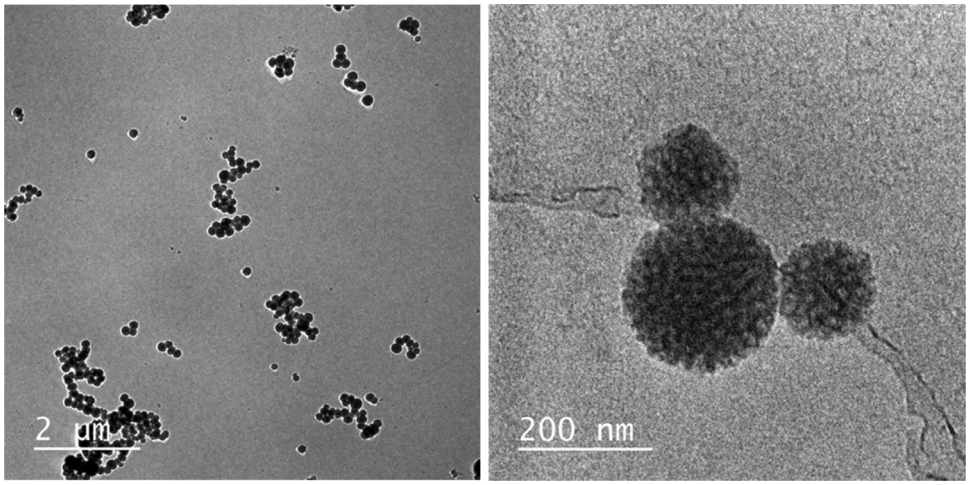

Fig. 1. Cryo-TEM of a sample from NMCS-containing 0.1 M NaOH solution.

production of graphene and graphite coated steel plates with high adhesion properties. In the carbon-based coated samples, the presence of a thin hematite (Fe_2O_3) layer on the outermost surface, with a magnetite (Fe_3O_4) layer underneath, was responsible for enhanced corrosion resistance [26]. Kirkland et al. [25] explained that, for pure metals, e.g. Cu and Ni, the carbon-based coating provides higher corrosion resistance because of the suppressed cathodic reaction ($2H_2O + O_2 + 4e^- \rightarrow 4OH^-$) in aerated chloride-containing solutions. The study attributed the reduced reduction rate to retardation of ionic transfer in the medium in the presence of the coating, i.e. increased corrosion resistance due to concentration polarization.

Carbon-based coatings have been extensively studied and used for improving the corrosion resistance of metallic bipolar plates, and employed in highly corrosive environments in fuel cell applications [32]. The dense and compact nature of the deposited carbon film was reported to be responsible for the high chemical stability and electrical conductivity of the plates [33]. Most of the reported studies on corrosion control by carbon-based materials have mainly focused on the barrier properties and general electrochemical response of the carbon-based coatings [28–33]. Detailed studies on the effect of carbon-based materials on the oxi/redox behavior of steel substrates and/or steel reinforcement, especially in contact with an alkaline environment, e.g. simulated concrete pore water, are limited.

In the framework of a line of research on corrosion control in reinforced concrete by using nanomaterials [34–36], nitrogen-doped mesoporous carbon spheres (NMCS) were considered and are the subject of this work. Porous carbon materials, such as NMCS, have huge potential applications in a wide range of fields, e.g. adsorption, energy conversion and storage, catalysis, and sensor technology, because of their unique characteristics, such as high surface area, large porosity, and good biocompatibility [37–39]. Bearing this in mind, the high surface area of the NMCS particles employed in this work (from 343 to 363 $m^2 g^{-1}$) [38] and their high porosity (from 0.45 to 0.48 $cm^3 g^{-1}$) [38], including the expected alteration in the electrical properties of the bulk (concrete) matrix in their presence, several hypothetical applications were aimed at. For example, NMCS-modified cement-based bulk matrix would theoretically present reduced electrical resistance. Hence, a possible application for NMCS in cement-based layers within cathodic protection systems, or in control of stray-current-induced corrosion in reinforced concrete, could be a novel and feasible approach. Preliminary results on admixing 0.025 wt.% NMCS (with respect to dry cement weight) in cement based materials [37] indeed showed a 15% decrease in the electrical resistivity of the mortar specimens, compared to control (admixture-free) mortar. These results indicated a potentially good performance for the modified matrix, if reinforced mortar or concrete are considered.

Prior to studies of NMCS-modified reinforced cement-based materials, the NMCS particles had to be evaluated with respect to their effect on the steel electrochemical response. To that end, this work reports on the influence of NMCS (internal pore size of 5.4–16 nm) on the electrochemical response of low carbon steel (St37) in model alkaline solutions with pH 13.9 and 12.8. The solutions were chloride-free or chloride contaminated in order to resemble steel in concrete pore water in control or corroding conditions. The paper concludes with recommendations on the application of NMCS in reinforced concrete, considering the drawbacks in the application of dispersing agents, as they are normally employed together with carbon-based admixtures.

2. Experimental materials and methods

2.1. NMCS preparation and characterization

The NMCS were prepared by using dopamine/polystyrene-*block*-poly(ethylene oxide) (DA/PS-*b*-PEO) composite micelles, with the full details on NMCS preparation as reported in [38]. In this case, dopamine was used as a carbon and nitrogen source, and PS_{173}-*b*-PEO_{170} micelles acted as the pore forming agent, which was subsequently removed by carbonization, so that the NMCS were produced with mesopores in the range of 5 to 16 nm and a mean particle size of ~200 to 300 nm [38]. Aiming at a homogeneous dispersion of NMCS in model solutions of 0.1 M and 0.9 M NaOH (pH 12.8 and 13.9, respectively), poly(ethylene oxide)-*block*-poly(propylene oxide)-*block*-poly(ethylene oxide) (PEO_{100}-*b*-PPO_{65}-*b*-PEO_{100}, Pluronic F127)) in a concentration of 10 wt.% was used as a dispersion agent [40,41]. A Cryogenic transmission electron microscopy (Cryo-TEM) image of a sample from the 0.1 M NaOH solution, containing NMCS, is presented in Fig. 1 for visualization purposes.

A Malvern Zetasizer Nano ZS90 was used to monitor the zeta potential of the NMCS in solutions in the relevant pH range, i.e. from 10 to 14, at 20 °C. The parent aqueous solution of 0.016 wt.% NMCS, with and without 10 wt.% F127, was corrected to the desired pH values by the addition of diluted solutions of NaOH or HNO_3. The zeta potential was measured separately in solutions with the following admixtures: i) 0.016 wt.% NMCS, ii) 10 wt.% F127, and iii) 0.016 wt.% NMCS +10 wt.% F127. Folded capillary zeta cells (DTS1070) were used. The zeta-potential values were measured by application of a low applied voltage gradient of 5 V.

2.2. Steel electrodes, model medium, and sample designation

Steel electrodes (low carbon St37) with an active surface area of 0.3 cm^2 were ultrasonically degreased in ethanol, ground with

Table 1
Sample designations and alkaline model solution composition.

Solutions	pH	NMCS/ wt.%	F127/ wt.%	Designation
0.1 M NaOH				
0% NaCl	12.8	0	0	A1
		0.016	0	A2
		0	10	A3
		0.016	10	A4
3.5% NaCl	12.5	0	0	A5
		0.016	0	A6
		0	10	A7
		0.016	10	A8
0.9 M NaOH				
0% NaCl	13.9	0	0	B1
		0.016	0	B2
		0	10	B3
		0.016	10	B4
3.5% NaCl	13.4	0	0	B5
		0.016	0	B6
		0	10	B7
		0.016	10	B8

successive grades of SiC emery paper up to 4000 grade, and then polished, using 3 µm and 1 µm diamond paste to achieve a mirror like surface. The electrodes were tested in model solutions of 0.9 M NaOH and 0.1 M NaOH with pH 13.9 and 12.8, respectively, at room temperature, ~ 20 °C. For each exposure condition, two identical steel specimens (replicates) were tested. Solutions with added NMCS were either dispersing agent-free, or additionally contained 10 wt.% F127 as a dispersing agent. The sample designations, corresponding to each studied environment, are given in Table 1.

2.3. Experimental methods

The progressive changes in the electrochemical response of the steel electrodes, when exposed to additive-free NaOH solutions and in the presence of additives (Table 1), were investigated during 72 h of immersion in 0.9 M and 0.1 M NaOH solutions with 0% and 3.5% NaCl. The duration of the test was chosen as a time interval sufficient for stable passive film formation in alkaline medium [2,7,15].

The corrosion potential (E_{corr}) and corrosion current density (i_{corr}), respectively, were recorded after 1 h, 24 h, and 72 h. The electrochemical response was studied in chloride-free model solutions and in the presence of 3.5% NaCl (Table 1), using a common, three-electrode flat cell with its geometry and set-up as previously reported [37], where a saturated calomel electrode (SCE) was used as the reference electrode, and mixed metal oxide (MMO) Ti mesh was used as the counter electrode.

The electrochemical measurements were executed using a Metrohm Autolab PGSTAT302. The polarization resistance of the treated steel samples was derived by linear polarization resistance (LPR) measurements in the potential range of ± 20 mV vs. E_{OCP} with a scan rate of 10 mV/min. The corrosion current density (i_{corr}) was calculated by using the Stern-Geary equation [39], $i_{corr} = B/R_p$, where R_p is the polarization resistance and B is the Stern-Geary constant. The value of $B = 26$ mV for active carbon steel was used and 52 mV for passive steel [42–44]. Electrochemical impedance spectroscopy (EIS) was performed at OCP, from 10 kHz down to 10 mHz. An AC perturbation voltage signal of 10 mV (rms) amplitude was applied. Replicates from all sample groups were subjected to cyclic voltammetry (CV) measurements after 72 h of exposure to the alkaline model solutions with pH 13.9 and 12.8. Ten CV cycles were recorded from −1.2 V to +0.9 V vs. SCE at a scan rate of 1 mV/s.

At the latest studied time interval (72 h), the steel surface was analyzed for morphological features (appearance) after treatment, using Environmental Scanning Electron Microscopy (ESEM), Philips-XL3 under accelerating voltage of 20 kV in low vacuum mode. The specimens were taken-out from the relevant solutions, dried-out by compressed air and placed in the vacuum chamber of the instrument. The micrograpahs are for visualization purposes and as supportive information only.

3. Results and discussion

3.1. NMCS characterization in model medium

In view of the global corrosion resistance of steel in alkaline solutions, changes in the surface charge of the admixed NMCS would account, or be responsible, for certain alterations in the steel electrochemical response. Consequently, the zeta-potential of the NMCS particles was considered to be an important parameter in this work. The zeta-potential values of the NMCS particles were measured in NaOH at pH from 10 to 14 and the obtained values are given in Table 2.

Analysis of the results in Table 2 leads to the conclusion that, in the pH range from 10 to 14, the zeta-potential values for NMCS particles in the tested solutions can be classified into two main domains; i) pH 10–12, and ii) pH 13-14. For the first pH domain (pH from 10 to 12), the NMCS particles were negatively charged. Increasing the pH of the solutions from 10 to 12 was accompanied by reduced negative charge. In this case, the highest negative zeta potential was measured at pH 11. In solutions with pH > 12, i.e. at pH 13 and pH 14, positive zeta potential was recorded for the NMCS particles. Taking into account the mechanism of measuring zeta potential using the Malvern equipment, i.e. by application of a low voltage gradient between cell electrodes (5 V), hydrogen and oxygen evolution on the cell electrodes are expected to be enhanced at pH 13 and 14, since these are media with already significantly increased ionic strength and conductivity, respectively. In other words, the cuvette and internal electrodes act as an electrochemical cell, where the applied voltage brings about pronounced oxidation and reduction reactions, which are also catalyzed by the NMCS particles. All these factors have certainly affected the measured zeta-potential values at the highest pH values. This fact explains the observed sharp changes in the measured values. If the same error is considered in all the tested solutions, however, a comparison of surface charge behavior is possible, if taken as such, rather than accounting for absolute values.

Some authors [45–47] argue that nitrogen-adjacent carbon atoms in the NMCS skeleton are positively charged and act as active sites for the adsorption of oxygen and/or negatively charged species such as OH^-, which could explain the negative charge of NMCS species in alkaline solutions with pH from 10 to 12, as shown in Table 2. Possible hydroxyl ion sorption on N-doped carbon surfaces in alkaline solution has been confirmed and reported [47]. This process precedes a quick and reversible two-step charge-transfer process, as shown in Eqs. (1) and (2). In this case, the hydroxyl sorption process leads to the accumulation of electrons on the NMCS surface [47], which could explain the reason for the NMCS negative charge density.

$$* + OH^- \leftrightarrow * - OH_{ads} + e^- \quad (1)$$

Table 2
Zeta potentials of NMCS in NaOH solutions with pH from 10 to 14 at 20 °C.

NaOH	pH 10	pH11	pH 12	pH 13	pH 14
zeta-potential (mV)	−38.1 ± 1.4	−42.5 ± 0.7	−34.2 ± 0.9	6.2 ± 2.4	35.6 ± 3.1

$$* - OH_{ads} + OH^- \leftrightarrow * - O_{ads} + H_2O + e^- \quad (2)$$

The hydroxyl sorption process was reported to be more predominant in solutions with pH from 7 to 11 [47], resulting in negative charge. In line with these considerations, negative zeta-potential values were measured for the NMCS at pH 10 and 11, as shown in Table 2. It has been also reported [47] that increasing the [OH^-] concentration has a significant effect on the electron transfer number. The electron transfer number will decrease as a function of [OH^-] increase. Consequently, in highly alkaline solutions (pH 13 and 14), the measured positive charge of NMCS particles could be explained by the potential variation of nitrogen-oxygen surface active functional groups, e.g. hydroquinone-/quinone- like groups on NMCS.

This type of variation of the nitrogen-doped sites on the carbon spheres is pH-dependent, which could induce considerable changes in the global corrosion resistance and the electrochemical response of the steel, when treated in the presence of NMCS.

3.2. Corrosion potential (E_{corr}) and corrosion current density (i_{corr})

The corrosion potential (E_{corr}) and the corrosion current density (i_{corr}) for all tested steel electrodes were recorded under all conditions in the course of continuous exposure to 0.1 M and 0.9 M NaOH solutions with different additives. The obtained results are displayed in Figs. 2 and 3. Figs. 2 and 3 also show the threshold (both potential and current) for steel passivity (or the steel active state, respectively), i.e. for an alkaline medium with or without chloride ion contamination, −270 mV vs. SCE for the corrosion potential and 0.1 μA/cm^2 for the corrosion current density, are the generally accepted thresholds [2,6,7,10].

As information, supportive to the discussion on the electrochemical response and the derived parameters, Figs. 4 and 5 in this section present visual observations (ESEM micrographs), taken on the steel surface after 72 h of treatment in presence of chloride. As a supplementary information, the ESEM micrographs for chloride free samples (A1–A4 and B1–B4) are listed, Figs. S1 and S2.

3.2.1. Control cases - chloride-free solutions

In chloride-free solutions of 0.1 M NaOH, pH 12.8 (samples A1 to A4), more anodic E_{corr} values were measured, shifting within the range of −200 mV to −100 mV at the end of the test (Fig. 2a). In line with this ennoblement, the i_{corr} values for specimens A1 to A4 stabilized at low current densities, well below the threshold of 0.1 μA/cm^2 after 72 h of treatment (Fig. 2a). This variation in E_{corr} and i_{corr} was as expected and is related to the formation of an electrochemically stable passive film on the tested steel in an alkaline environment with pH 12.8. Although similar mechanisms would hold for the steel tested in 0.9 M

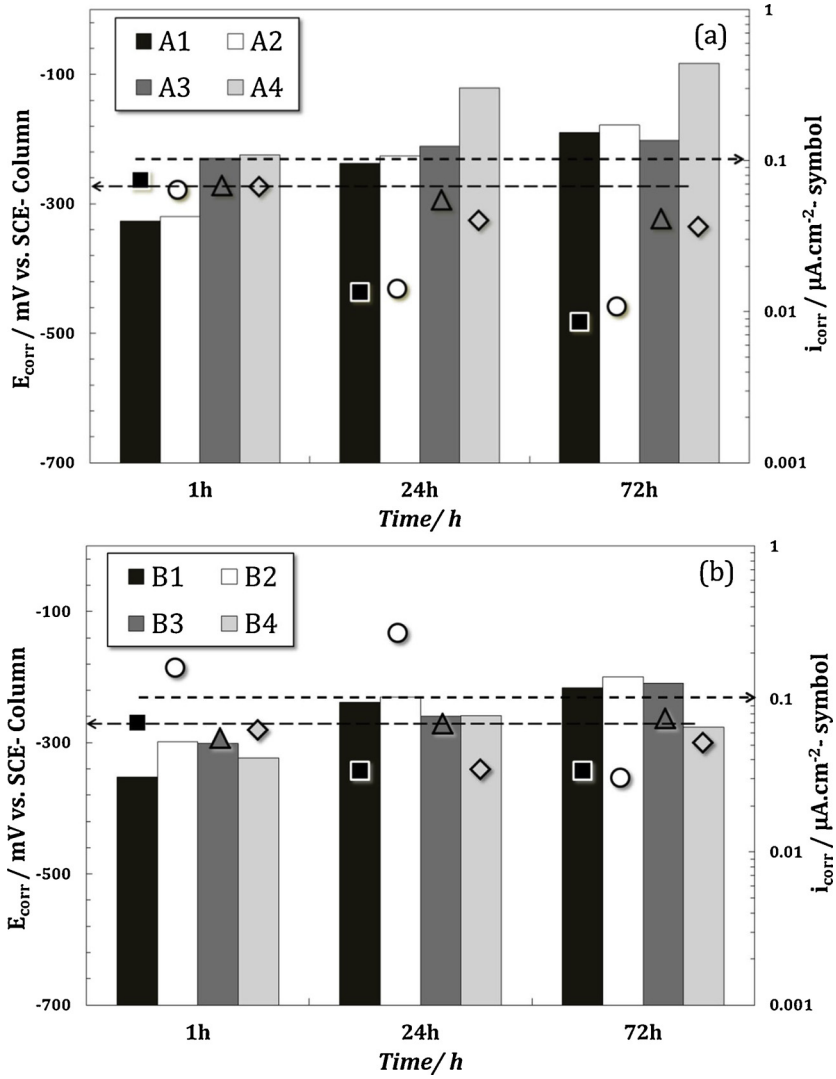

Fig. 2. Corrosion potential (E_{corr}, column) and corrosion current density (i_{corr}, symbols) for steel in chloride-free solutions: (a) 0.1 M NaOH (A1–A4), and (b) 0.9 M NaOH (B1–B4).

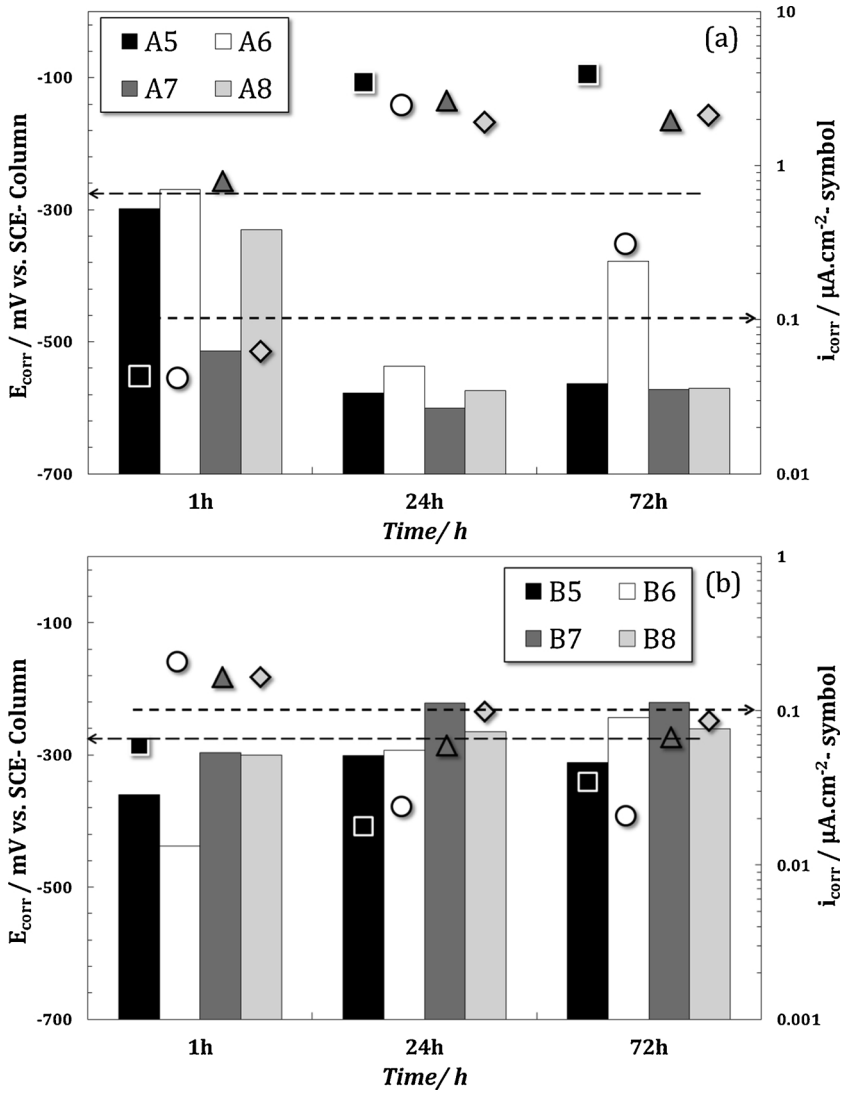

Fig. 3. Corrosion potential (E_{corr}, columns) and corrosion current density (i_{corr}, symbols) for steel in chloride-containing solutions: (a) 0.1 M NaOH (A5–A8); (b) 0.9 M NaOH (B5–B8).

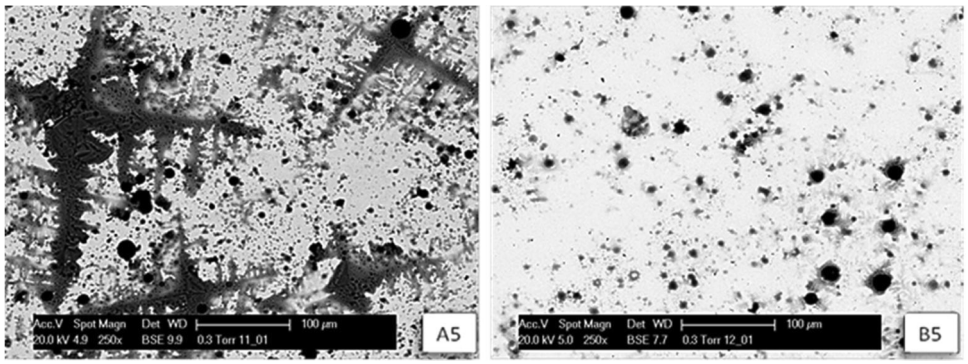

Fig. 4. ESEM micrographs, magnification 250× – steel surface after 72 h treatment *in chloride-containing and additives-free:* 0.1 M NaOH (A5) and 0.9 M NaOH (B5).

NaOH, pH 13.9 (B samples), more cathodic E_{corr} values were recorded for these specimens throughout the test (B1 to B4), accompanied by slightly higher i_{corr} values, (Fig. 2b). This is related to an initially active steel surface at pH > 13.7. In what follows, the evolution of corrosion potentials and corrosion current densities for the steel electrodes in chloride-free (control cases) and chloride-containing (corroding cases) 0.1 M and 0.9 M NaOH solutions will be discussed in more detail per specimens' group and relevant conditioning, *with an emphasis on the effects of NMCS* particles *and/or the dispersion agent F127*.

3.2.1.1. Chloride-free 0.1 M NaOH solutions (Fig. 2a). For chloride-free solutions of 0.1 M NaOH (designation A), the presence of 0.016% NMCS (specimen A2) and/or 10% F127 (specimens A3, A4) induced a relatively more anodic E_{corr} potential with respect to the solutions

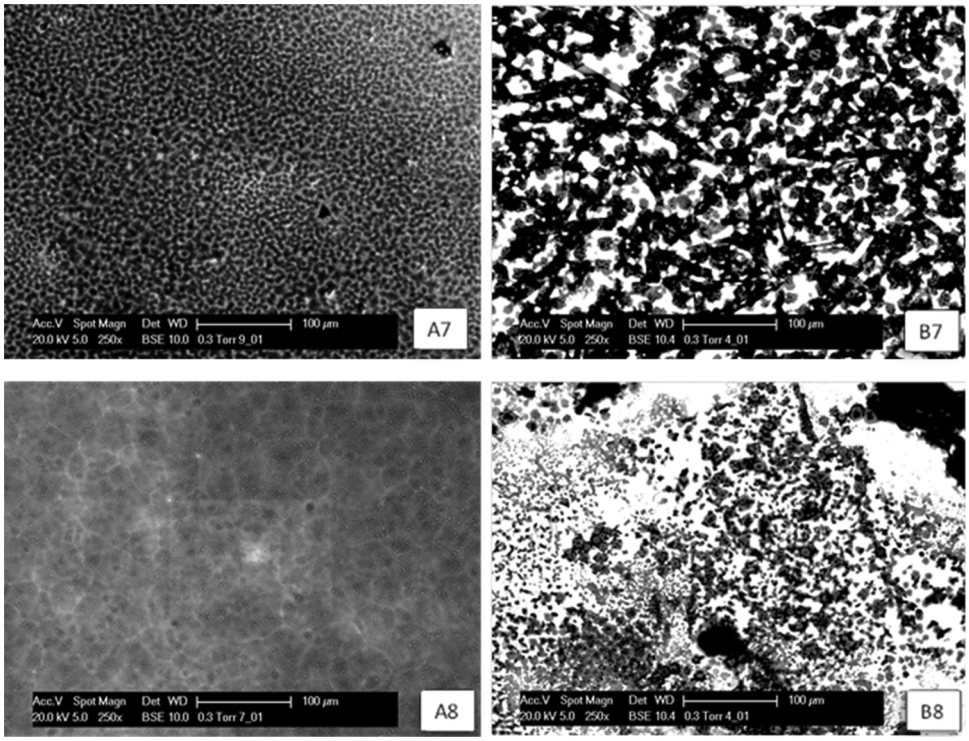

Fig. 5. ESEM micrographs, magnification 250× – steel surface after 72 h treatment *in chloride-containing* 0.1 M NaOH (A7, A8) and 0.9 M NaOH (B7, B8) with additives: A7 and B7 – F127 only; A8 and B8 – NMCS + F127.

without additives (A1). These anodic E_{corr} values were more pronounced for the steel treated in F127-containing solutions at the beginning of the test (specimens A3 and A4) and after 24 h and 72 h in the presence of 0.016% NMCS + 10% F127 (specimen A4), and 0.016% NMCS only (specimen A2), specifically for the former case (A4 in Fig. 2a).

It should be noted that, although specimen A4 exhibited the most noble potential compared to all the other cases, a larger current density was observed (Fig. 2a). Fundamentally, the anodic shift in E_{corr} and the low i_{corr} values measured in all cases, including those where 0.016% NMCS were present (A2 and A4 specimens), indicate the passivation of the steel electrodes and the development of an electrochemically stable oxide film, as expected and previously reported elsewhere [6,15,48]. Compared to the control, additive-free conditions (A1), however, the more noble potentials but higher current densities for A2 and A4 deserve attention. The presence of NMCS in the medium was relevant to both the A2 and the A4 cases. Therefore, the differences in electrochemical response for these samples can be attributed to the presence (samples A4) or absence (sample A2) of the dispersing agent F127. For comparison purposes, in sample A3 only F127 was present in the solution. Next, an incomplete dispersion of NMCS particles could have been relevant for A4, while pronounced sedimentation of NMCS particles could have been involved in the A2 solutions in the course of treatment. Hence, only particles adhering to the steel surface, in the immediate vicinity of the steel/solution interface or, at the very minimum, floating in the bulk volume of the solutions, would be responsible for the observed steel response in the case of samples A2, A3, and A4. In fact, as can be seen in supplementary information Fig. S.1, ESEM observations for the steel surface, treated in chloride-free NMCS-containing solutions (A2, A4) reveal similar appearance, with features denoted to potentially adhered NMCS.

As can be seen in Fig. 2a, at the initial time interval of 1 h, the E_{corr} indicates a more pronounced effect of particle interaction on the steel surface in solutions where F127 was present – samples A3 and A4. This was reflected by their more noble potentials after 1 h of treatment. The effect of NMCS alone, as in sample A2, was not obvious at this stage. The effect of F127, however, seemed to be a barrier effect, rather than an effect on the oxidation/reduction reaction mechanism, since the derived corrosion current densities for the A3 and A4 samples remained similar to those for the control, A1 case. After 24 h of treatment and onwards, the effect of F127 was not significant and potentially even negative: the E_{corr} for the A3 specimens remained similar to its initial value, while its corrosion current density values remained stable, but higher than for the A1 specimens (Fig. 2a). This suggests a barrier against the formation of an electrochemically stable passive film, such as obviously formed in the A1 specimens, possibly due to the F127 interference in A3 specimens. In contrast, the effects of NMCS particles, alone or together with F127, became more pronounced within the course of treatment: ennoblement was observed for specimens A2 and A4, but was more significant for A4 specimens (Fig. 2a). The positive effect of NMSCs alone can be clearly observed, since the E_{corr} noble shift was accompanied by lower current densities (A2 specimens, Fig. 2a).

Although similar performance was observed for A4, the most noble potential for this specimen at the end of the test was not in line with the higher current density. This result involves an apparent counterbalancing effect between NMSCs and F127, so far as passive layer formation and stabilization are concerned, i.e. positive effect of NMSCs and "negative" effect of F127. In other words, the higher anodic shift in the E_{corr} values for the A2 and A4 specimens at the end of the test resulted from the effects of the NMCS particles on the oxidation/reduction reactions on the steel surface. For the former case, A2, the NMCS alone were responsible for the observed performance (compared to the A1 control sample), while in the latter case, i.e. A4, an interaction between the NMCS and F127 most likely occurred. This effect also follows the reversible charge-transfer process on the particles' surfaces, as discussed in Section 3.1, which contributes to the passive layer formation in A2 and is counterbalanced by F127 in the case of A4. Consequently, in case of A4, an adsorbed composite layer of F127 and NMCS obviously altered the electrochemical properties of the passive film that was formed, compared to the case of A2 (different surface morphology was clearly observed by ESEM, Fig S.1). Potential blocking of the cathodic sites and limitation of the reduction process were

expected in both the A2 and the A4 specimens, which explains the anodic shift in the corrosion potential, as shown in Fig. 2a. This shift in the potential after 24 and 72 h was not observed in the case of the A3 sample where only F127 was present in the medium (Fig. 2a) and is, in fact, supported by ESEM observations (Fig. S.1), where a relatively "clean" surface and no evidence of adhered F127 was observed in the case of A3 after 72 h of treatment.

3.2.1.2. Chloride-free 0.9 M NaOH solutions (Fig. 2b). Detailed analysis of the E_{corr} and i_{corr} values in chloride-free 0.9 M NaOH solutions (pH 13.9, designation B, Fig. 2b), indicated that for steel treated under the additive-free, control conditions (B1), the most cathodic E_{corr} potential was initially observed (Fig. 2b, B1). After 72 h, ennoblement was recorded for specimens B1, B2, and B3, for which similar values around −200 mV were recorded. In the presence of both 0.016% NMCS and 10% F127, a relatively more cathodic E_{corr} potential was measured for sample B4 (Fig. 2b). The highest corrosion current density was initially recorded for the case of steel treated in solution B2, with 0.016% NMCS only. These values were the highest among all tested specimens up to 24 h of immersion. After 3 days, however, sample B2 showed low i_{corr} that was similar to that of the additive-free control case B1. In fact, the most noble potential, in line with the lowest corrosion current density values, was recorded for sample B2 at the end of the test. In contrast, higher i_{corr} values were recorded after 72 h in the case of samples B3 and B4, an observation similar to the already discussed one for the case of A3 and A4 in solutions with pH 12.8, as shown in Fig. 2a. Here again, the positive effect of the NMCS particles alone was evident, and especially pronounced with longer treatment. This delay in the positive effect of NMCS particles in both 0.1 M and 0.9 M solutions accounts for their effect in view of the altered electrochemical reactions on the steel surface, rather than just barrier effects or bulk solution modification, as is most likely relevant for the F127-containing solutions.

The effect of pH alone on the adsorbed layer on the steel surface, as well as on the electrochemical response in the presence of NMCS and F127, can be clearly observed by comparison of the E_{corr} potentials and i_{corr} values of the treated steel in the 0.1 M NaOH (A4) and 0.9 M NaOH (B4) solutions. In alkaline solutions with pH 13.9 (B4), more cathodic E_{corr} and higher i_{corr} values were registered than in case of specimens A4 (pH 12.8). This indicates that the pH difference between the two solutions is responsible for changes in the properties of the oxide layer, including the contribution of F127 and altered NMCS properties (Section 3.1), which is consequently reflected in the steel electrochemical response.

If a comparison of surface appearance is made between control specimens (Figs. S.1 and S.2), the following can be noted: Fig. S.1 depicts a surface modification in the case of A4 specimens (if compared to additives-free A1 specimens), denoted to the presence of NMCS + F127, with (perhaps selectively) adhered NMCS to cathodic areas (bearing in mind that in 0.1 M NaOH, the NMCS were negatively charged). In contrast, the steel surface in specimens B4 presents a more significant surface alteration, potentially a larger accumulation of NMCS (agglomeration or larger quantity of these), which would be adhered to the anodic sites. Considering that the steel surface was initially more active in 0.9 M NaOH (as previously discussed and also reflected by the results in Fig. 2), a larger active (anodic) surface would determine a larger accumulation of NMCS-containing product layer, as actually observed in Fig. S.2 for B2 and B4 specimens, if compared to the surface appearance in A2 and A4 specimens, Fig. S.1.

It has been reported that the reduction of Fe^{3+} to Fe^{2+} constitutes an additional cathodic reaction, which logically affects the evolution of E_{corr} potentials and i_{corr} values [10,15,49]. The contribution of Fe^{2+} species is expected to be more evident when the steel potential shifts to more negative values [49]. Consequently, for the steel performance in this work, the high i_{corr} values in 0.9 M NaOH solutions (B1 sample) can be also related to the accumulation of Fe^{2+} species within the passive film. When the steel was exposed to solutions with lower pH, however, which was the case for the 0.1 M NaOH solution (sample A1), the more anodic E_{corr} and lower i_{corr} values could be related to enrichment of the passive film in Fe^{3+} oxides/hydroxides [10,49]. This is in addition to the previously discussed NMCS-triggered limitation of the reduction reactions on the steel surface at this pH, consequently also limited Fe^{3+} to Fe^{2+} reduction. Considering the expected hydroxyl sorption processes accompanied by electron transfer processes [47], following Eqs. (1) and (2), the cathodic shift in E_{corr} potential in the presence of 0.016% NMCS + 10% F127 (B4) could be explained by the effect of NMCS on the Fe^{3+} to Fe^{2+} reduction process. This cathodic shift in the E_{corr} potential was not observed in the B3 solution with only F127. On the other hand, the decrease in i_{corr} values for the treated steels with immersion time in B4 cases would be related to the barrier effect of the adsorbed layer on the steel surface, together with the NMCS interference due to their attraction at anodic locations.

In addition to the above considerations, the behavior of F127 in the two different solutions deserves to be briefly pointed out. Although F127 was used as a dispersing agent only, hence not a subject of primarily interest and discussion, its presence in the medium would affect the electrochemical response. It has been reported that the micellization and adsorption behavior of Pluronic F127 block copolymers on hydrophobic surfaces are pH sensitive, specifically in the presence of NMCS [45–48,50]. This will determine the dispersion efficiency of F127 in both 0.1 M and 0.9 M NaOH. In 0.9 M NaOH (pH 13.9), the solubility of F127 is reduced, resulting in an increase of the micellization degree [50,51]. This determines a lower number of copolymers, left to stabilize the NMCS particles, leading to agglomeration of NMCS. In contrast, for solutions of 0.1 M NaOH (pH 12.8), F127 is reported to present a lower micellisation degree [51]. Therefore, the adsorption of this nonionic surfactant (F127) on the surface of NMCS particles in 0.1 M NaOH will result in improved dispersion of NMCS.

Consequently, for specimens B4, accumulation of agglomerated, or a large number of, particles would be expected as part of the product layer on the steel surface, as in fact observed, Fig. S.2 (F127 only would be seen as "worm-like" features on the surface, as also observed for specimens B3). In contrast, for specimens A3 and A4, the NMCS would be better dispersed, leading to a (potentially) uniform distribution in the product layer on the steel surface. This was as observed as well, Fig. S.1, where the distribution of features of smaller dimensions was evident in the presence of NMCS + F127 (specimens A4). The better dispersing effect of F127 in 0.1 M NaOH is also well seem, if specimens A2 and A4, Fig. S.1 are compared versus the surface appearance of specimens B2 and B4 (Fig. S.2). Additionally, the higher solubility of F127 at pH 12.8 and reduced micelle formation would account for the presence of F127 mostly in the bulk of the solution (F127 co-polymer chains, unimers, including di-block co-polymer impurities), rendering minimum or none surface attraction of the polymer to the steel surface. A relatively clean steel surface in the case of A3 specimens (Fig. S.1), where F127 only was present in the solution, supports these considerations.

3.2.2. Corrosion cases - chloride-containing solutions

For the case of chloride-containing 0.1 M and 0.9 M NaOH solutions (with 3.5% NaCl), the measured E_{corr} and i_{corr} of carbon steel in the presence of different additives are shown in Fig. 3. The appearance of the steel surface after 72 h treatment in presence of chloride additives is presented in Figs. 4 and 5 (micrographs for specimens A6 and B6 are not available).

In chloride-containing 0.1 M NaOH, pH 12.5 (samples A5 to A8) and 0.9 M NaOH, pH 13.5 (samples B5 to B8), the steel corrosion resistance varied more significantly in time and with respect to the medium, as expected and if it is compared to the control conditions in Fig. 2. Visual observations, Figs. 4 and 5, also confirm the already altered surface properties of these samples i.e. a more significant product layer accumulation (including, where relevant, F127- and NMCS- containing

corrosion products) for specimens A5 to A8 and B5 to B8, if compared to the control, non-corroding conditions (A1 to A4 and B1 to B4).

The corroding "A" specimens in additives-free 0.1 M NaOH (A5) and in the presence of NMCS (A6, A8 in Fig. 5a) had an initially (after 1 -h immersion) higher corrosion resistance than the corresponding B specimens (B5, B6, B8 treated in 0.9 M NaOH, Fig. 3b). This variation in the initial corrosion response was similar to the trend observed for the chloride-free media (Fig. 2) and is attributed to the effects of pH, together with the presence of chloride ions as a corrosion accelerating factor.

For the case of pH 12.8 (A specimens), the oxide layer was electrochemically more stable, so that a delay in corrosion was expected. While there was an initially more active state of the film at pH 13.9 [8,10] in the B specimens, which resulted in a faster corrosion initiation. After 24 h, however, and until the end of the test, opposite performances were observed for the A and B specimens and are discussed below.

3.2.2.1. In chloride-containing 0.1 M NaOH, pH 12.5 (samples A5–A8, Fig. 3a). The onset of steel corrosion was detected after 24 h treatment for all cases, except for the case of A7 (solution containing F127), where the active state was recorded even earlier, i.e. within 1 h of treatment. This observation accounts for the negative effects of F127 on the steel electrochemical response, since the additive-free case (A5) and the NMCS-only case (A6) presented behaviour similar to that in the control (Cl-free) conditions (Fig. 2a). With prolonged treatment, the chloride-induced corrosion counteracted the formation of a passive film, in the otherwise alkaline medium, as reflected by a significant (cathodic) drop in potential to around −550 mV vs. SCE and an increase in corrosion current density values. The highest corrosion current density of approximately 4.3 μA/cm^2, well beyond the passivity threshold, was observed for the case of additives-free solution (A5), followed by the F127-containing cases (A7 and A8), Fig. 3a. It should be noted that, towards the end of the test, 72 h for specimen A6 (NMCS alone), there was an improvement in the corrosion resistance, confirmed by ennoblement of the potential and reduced current density to below 0.5 μA/cm^2. Obviously, there was an NMCS-induced positive effect on the steel corrosion resistance in Cl-containing alkaline medium. This can be explained by a possible trapping of chloride ions in the porous matrix of the NMCS (undispersed in this case) particles, due to adsorption of negatively charged species on the positively charged nitrogen-adjacent carbon atoms. The most cathodic (active) potentials were recorded for A7 and A8, accompanied by high corrosion current densities (Fig. 3a). This result is related to the possible accumulation of chloride ions in the corrosion product layer, that is developing on the steel surface, trapping the chloride ions within the adsorbed polymer itself, while blocking the active surface of the NMCS particles by F127. All these lead to a reduced efficiency of the NMCS-triggered positive action. The ESEM micrographs support the above considerations, showing a relatively uniform (corrosion) product layer, deposited overall on the surface of both A7 and A8 specimens, Fig. 5. In contrast, the surface of A5 specimen (treated in additives-free medium), Fig. 4, presents a significantly larger in scale but non-uniform corrosion damage (as would be expected within Cl-induced corrosion), and together with well observable salts crystallization on the steel surface. This is also well in line with the highest, among all recorded, current density values for specimen A5 at the end of the test (Fig. 3a).

3.2.2.2. In chloride-containing 0.9 M NaOH, pH 13.4 (Fig. 3b). The presence of 0.016% NMCS induced a significant cathodic shift in E_{corr} and higher i_{corr} values at early stages (sample B6) compared to the additive-free case (sample B5); a more active state in view of corrosion currents was also observed for the samples treated in both F127 alone and for NMCS + F127 containing solutions (B7 and B8 specimens, Fig. 3b). In contrast to specimens A5 to A8, after an initially more active state, specimens B5 to B8 exhibited the reverse trend. After 24 h, the E_{corr} values for B5 to B8 shifted to significantly more noble values than for specimens A5 to A8, which maintained around the passivity threshold of −250 to −300 mV at the end of the test, as shown in Fig. 3b. In line with these E_{corr} values, the corrosion current density for specimens B5 to B8 was reduced to below the threshold of 0.1 μA/cm^2 after 24 h of treatment and remained low at the end of the test. In other words, the corroding B samples showed the same performance as the control ones, i.e. corrosion was initiated but was not sustained and did not propagate for specimens B5 to B8 (Fig. 3b). The anodic shift in the E_{corr} values and reduced corrosion current densities for steel samples B6 to B8 were associated with the blocking of the active steel surface by NMCS and/or F127. In these cases, the i_{corr} values reached values that were similar to, or even lower than (e.g. B6 at 72 h), those for the parallel chloride-free solutions (B2-B3), as shown in Fig. 2b. This response for steel in chloride-containing 0.9 M NaOH can be explained by the lower $[Cl^-]/[OH^-]$ ratio compared to that in 0.1 M NaOH with equal chloride content. For the former case, the already altered pH from 13.9 to 13.4, together with the lower critical chloride concentration at the steel surface, resulted in cessation of the corrosion propagation process. In the latter case, however, the pH changes from 12.8 to 12.5 and higher $[Cl^-]/[OH^-]$ ratio resulted in corrosion propagation.

The ESEM surface analysis for specimens B5, B7 and B8 (Figs. 4 and 5), presents features, in fact similar to the control cases in the B groups (Fig. S.2). The initiation of corrosion damage in B5 can be well observed as a variance to the B1 specimen, Fig. S.2. However, corrosion propagation and significant products accumulation was ceased, evident by minimal corrosion damage in B5, if surface appearance is compared to that in e.g. A5, Fig. 4. For the steel treated in F127-containing (B7) and NMCS + F127-conatining (B8) solutions, the surface is obviously covered by large amounts of product layer, both F127 and NMCS-containing. This accumulation is similar to the cases of A7 and A8, however it is of distinctively different morphology, implying a potentially different mechanism of product layer formation. Judged from the electrochemical response of B7 and B8 at the end of the test, together with the above considerations on the $[Cl^-]/[OH^-]$ ratio for the case of B specimens, these product layers are not expected to be chloride-ions rich. In contrast, they most likely caused limitations towards further corrosion propagation, resulting in the as observed increased corrosion resistance of B7 and B8 at the end of the test.

The above results and discussion on the overall electrochemical state of the steel electrodes under all tested conditions are supported and elucidated by qualitative analysis of the electrochemical impedance spectroscopy response and later-on, by cyclic voltammetry tests, which are presented and discussed below.

3.3. Electrochemical impedance spectroscopy (EIS)

EIS tests were performed for all tested specimens at time intervals, identical to the previously presented for E_{corr} and i_{corr} records. Figs. 6–9 present the EIS experimental response as an overlay of 1 h, 24 h and 72 h of treatment.

The obtained EIS data was fitted by the same equivalent electrical circuit (EEC), used in the previous work [37]. The EEC consisted of two hierarchically arranged time constants in series with the electrolyte resistance, i.e., $R_e(R_1Q_1(R_2Q_2)$, where R_e is the solution resistance; the high frequency time constant ($R_1{\cdot}Q_1$) is associated with the charge transfer resistance and pseudo-double layer capacitance; the low frequency time constant ($R_2{\cdot}Q_2$) is related to the redox transformations, mainly Fe^{2+}/Fe^{3+}. The global polarization resistance (Rp) values can be derived from EIS via simplification, using the relation of $R_p = R_1 + R_2$ [37]. The comparison of R_p data obtained by fitting EIS response and LPR is presented in Fig. 10 for both 0.1 and 0.9 M NaOH chloride-free solutions and in presence of 3.5% NaCl.

Figs. 6 and 7 present the EIS response for the control cases

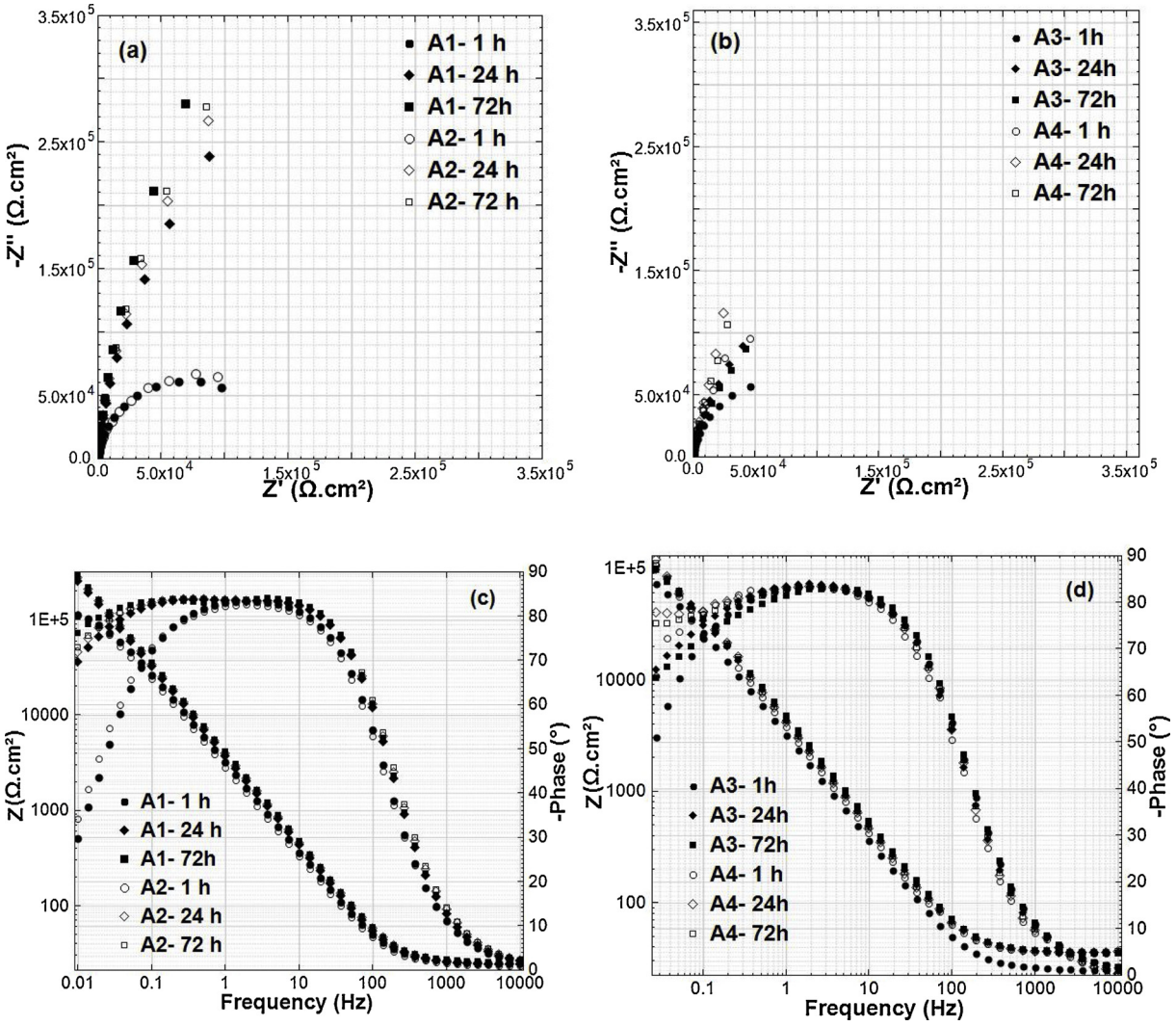

Fig. 6. Overlay of Nyquist (a,b) and Bode (c,d) diagrams of carbon steel after 1, 24 and 72 h of immersion in chloride-free A1–A2 and A3–A4 solutions.

(specimens A1 to A4 and B1 to B4). In control, 0.1 M and 0.9 M NaOH solutions without additives (A1 and B1, respectively), the limit of impedance values in the low frequency domain (towards 10 mHz) increases with immersion time (Figs. 6 and 7). This is related to the spontaneous passivation of steel in alkaline media. These observations are in line with the recorded evolution of the i_{corr} and E_{corr} values for specimens A1 and B1 with time of treatment, as depicted and previously discussed with relevance to Fig. 2. If the effect of pH is considered in control and additives-free solutions, the specimens A1 (pH 12.8) exhibit higher magnitude of impedance (Figs. 6a,c and 10 a), compared to specimens B1 (pH of 13.9, Figs. 7a,c and 10 b). This confirms the previously discussed hypothesis for a more electrochemically stable passive film in conditions of pH 12.8, resulting from predominance of Fe^{3+} species which induced the formation of passive films with higher polarization resistance R_p values (Fig. 10a,b). Furthermore, the higher stability of the passive layer on the steel surface in A1 is evident from the already more pronounced increase of impedance magnitude towards the end of the test (72 h) if compared to the EIS response for specimens B1 (compare A1 and B1 responses in Figs. 6a, c and 7 a, c and R_p fitting data Fig. 10a,b). The surface morphology of the steel electrodes (recorded by ESEM) did not show and distinguishable variation between A1 and B1 specimens, but rather a relatively clean steel surface for both cases was observed (Figs. S.1 and S.2), supporting the electrochemical response in view of passive state for these specimens.

In 0.1 M and 0.9 M NaOH solutions, where 0.016 wt.% NMCS were present (specimens A2 and B2), the observed EIS response after 1 h and 24 h of immersion was similar to that, recorded for specimens A1 and B1 (Figs. 6 and 7). However, after 72 h of immersion, the low frequency limits for both A2 and B2 was relatively lower, if compared to A1 and B1 specimens. The similarity in the EIS response in specimens A1-A2 and B1-B2 was mainly related to the non-complete dispersion of NMCS in the medium and/or the absence of F127. In contrast, the spontaneous passivation of steel in alkaline media in the presence of both NMCS and F127 (specimens A4 and B4) or F127 only (specimens A3 and B3) was limited and reasons for this performance was already discussed in Section 3.2. The impedance magnitude in these cases i.e. specimens A3-A4 and B3-B4 was lower, compared to the parallel cases of A1-A2 and B1-B2 (Figs. 6, 7 and 10). If the effect of F127 is to be studied with relevance to the EIS response, there was a clear increase in the overall impedance for the specimens A4 (NMCS + F127), compared to specimens A3 (F127 only), Fig. 6b, d. Similarly, the overall impedance for specimens B4 was significantly higher, if compared to the B3 specimens (F127 only, Fig. 7b, d). The EIS results are well in line with the results in Fig. 2, where the highest corrosion current densities were derived for specimens A3 and B3, if also compared to specimens A4 and B4.

In chloride-containing 0.1 M NaOH (Fig. 8), after 1 h, the overall impedance for specimens A5 to A8 substantially decreased with immersion time, with a clear depression of the phase angles, and in agreement with the Rp data (Fig. 10) and the recorded E_{corr} and i_{corr}

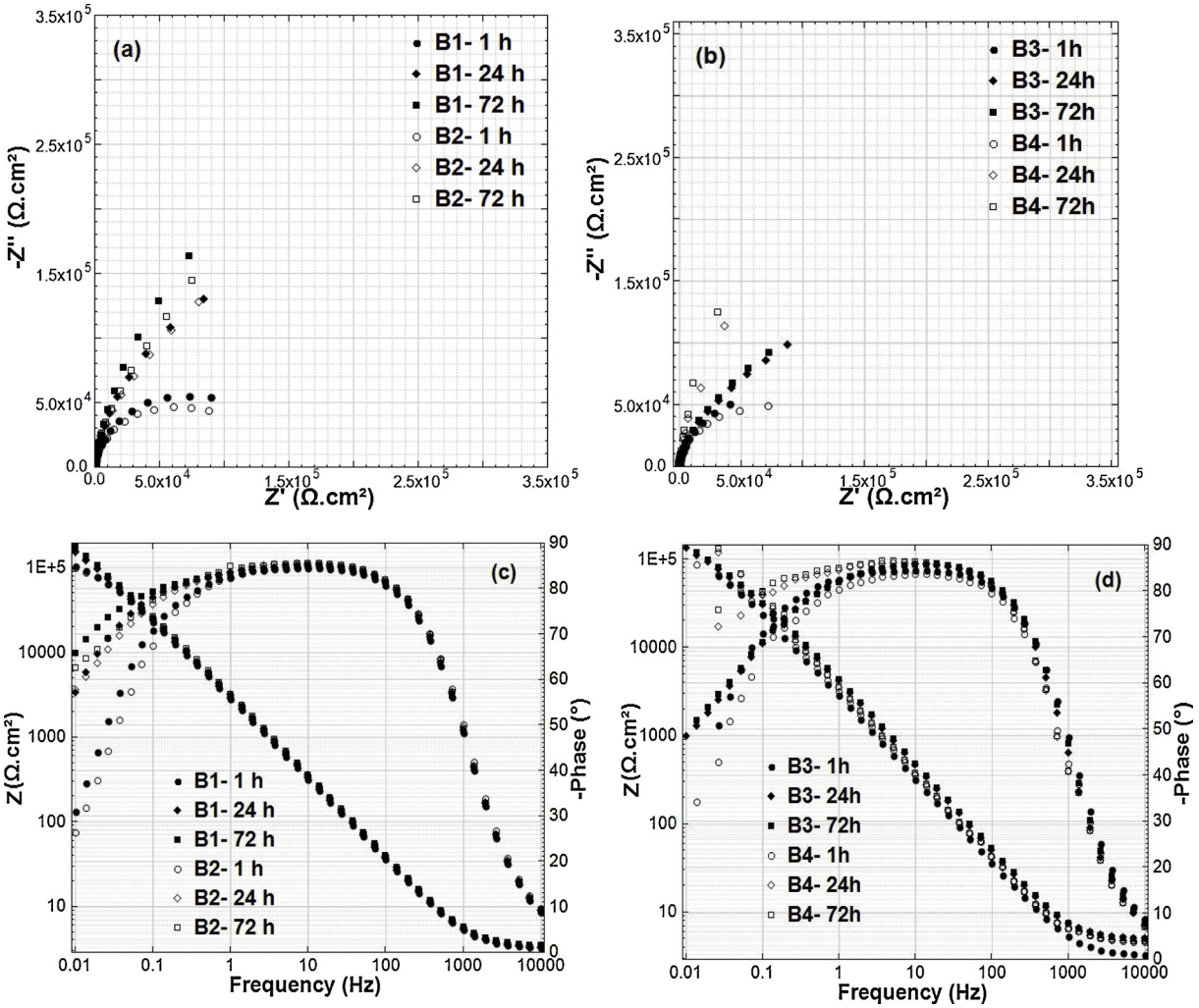

Fig. 7. Overlay of Nyquist (a,b) and Bode (c,d) diagrams of carbon steel after 1, 24 and 72 h of immersion in chloride-free B1–B2 and B3–B4 solutions.

values (Fig. 3).

The EIS response reflects the corrosion onset and corrosion propagation with time in A5 to A8 specimens in the presence of 3.5% NaCl and is well in line with the recorded, and previously discussed, E_{corr} and i_{corr} values (Fig. 3a). The EIS response for steel treated in NMCS only containing solutions (A6), showed an increase of corrosion resistance after 24 h and towards the 72 h of treatment, which is in line with the lowest recorded i_{corr} and most noble potential at the end of the test (Fig. 3a) and Rp fitting data shown in Fig. 10b. Detailed EIS analysis is not subject to this contribution. It can be noted, however, that in addition to purely electrochemical state, the EIS response (as well known) reflects well the surface properties of the steel specimens. Hence, supports the already discussed phenomena in corrosion product layer formation in all conditions. As seen in Fig. 8b,d, at 72 h, the corrosion resistance for steel, treated in Cl-containing solutions in the presence of both NMCS and F127 (A8 specimens) increased, reflected by a relatively high impedance magnitude at the low frequency limit and stabilized phase angle (Fig. 8b, d). This limitation of the corrosion process is not observable from the LPR tests, where the global state of the steel surface is reflected only. For the F127-containing medium (specimen A7), such limitations were not observed, but a continuous reduction only of corrosion resistance was evident in time of treatment (Fig. 8b, d). For the case of A7, a well-pronounced appearance of a second time constant in the EIS response at later time intervals (Fig. 8d) and lower corrosion currents (Fig. 3a) if compared to the A5 specimens, were relevant. For the case of A8, a second time constant is not well pronounced, and the product layer appears to be more homogeneous and uniform (Fig. 5), in contrast to the steel surface in A5, covered by a non-uniform corrosion product layer (Fig. 4). The different product layer morphology in specimens A7 and A8 (Fig. 5) was apparently responsible for their different corrosion performance.

Finally, for *chloride-containing 0.9 M NaOH*, (B5–B8 specimens, Fig. 9), a more capacitive-like behavior was monitored in time of treatment for some specimens, e.g. EIS response for B5 (Fig. 9a,c), remaining almost constant with treatment. The previously discussed effect of $[Cl^-]/[OH^-]$ ratio in the presence of additives (specimens B7 and B8) is also illustrated by increase and stabilization of the impedance magnitude towards the end of the test (Fig. 9b,d). Clearly, not only the accumulation of product layers in B7 and B8 (Fig. 5), but also the variance in their morphology, resulted in a limitation towards further corrosion propagation and improved corrosion resistance for these specimens, if compared to the A7 and A8 ones, treated in 0.1 M NaOH (Fig. 8). Moreover, the product layers in specimens B7 and B8 would be expected to be of a different composition, electron and ionic conductivity, if compared to the product layers in specimens A7 and A8, since a well pronounced second time constant for B7 and B8 was not observed (Fig. 7d). The EIS response for B5 to B8 specimens is clearly in line with the higher corrosion resistance for this group, as recorded by LPR tests (Figs. 3b and 10).

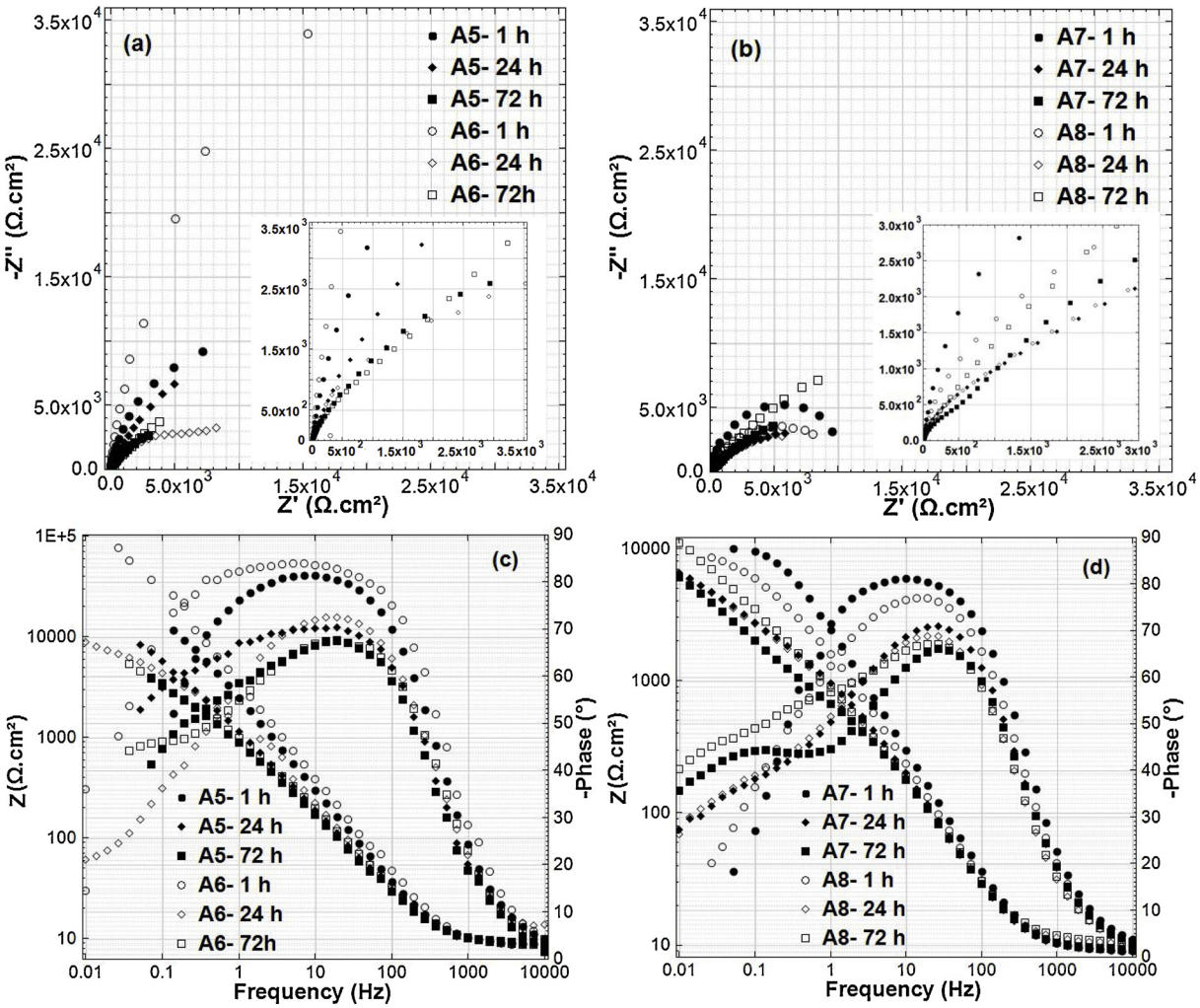

Fig. 8. Overlay of Nyquist (a,b) and Bode (c,d) diagrams of carbon steel after 1, 24 and 72 houres of immersion in chlorid-containing A5–A6 and A7–A8 solutions.

3.4. Cyclic voltammetry (CV)

The behavior of carbon steel in NaOH solutions with different pH, with and without chloride contamination and additives (i.e. NMCS and F127), was analyzed by performing CV after 72 h of treatment. The results below refer to a comparison of the steel response in control (chloride-free) solutions with pH 12.8 and pH 13.9 (specimens A1 to A4 and B1 to B4) and in the chloride-containing, high pH medium of 13.9 (specimens B5 to B8). This choice was made with the motivation of, on one hand, elucidating the unexpected performance in both alkaline solutions when no chlorides were present; and on the other hand, explaining the similarly unexpected, higher corrosion resistance of steel treated in an even higher pH (13.9) medium in the presence of chloride ions. The CV response for specimens A5 to A8 is not presented, since the outcome was, as expected, a significantly increased current density with cycling, entirely in line with the observed high current densities and cathodic potentials in this group, as discussed with relevance to Fig. 4a.

3.4.1. Response in chloride-free NaOH solutions (pH 12.8 and 13.9) under cycling

Fig. 11 presents an overlay of the 1st, 5th, and 10th CV scans for carbon steel in 0.1 M NaOH, pH 12.8 (specimen A1) and 0.9 M NaOH, pH 13.9 (specimen B1). Irrespective of the pH, three potential domains can be clearly distinguished: the iron redox process domain, the passivation region, and the oxygen evolution domain. At the most cathodic potentials in the forward scan, two main peaks, generally assigned to iron redox processes [11], can be distinguished: Peak I ($E \approx -0.95$ V vs. SCE) is associated with the formation of Fe^{II}-oxides, in accordance with Eqs. (3) and (4), [11]:

$$Fe + 4\ H_2O \leftrightarrow Fe(OH)_2 + 2H_3O^+ + 2\ e^- \quad (3)$$

$$Fe + 3\ H_2O \leftrightarrow FeO + 2H_3O^+ + 2\ e^- \quad (4)$$

Peak VI ($E \approx -1.1\ V_{SCE}$) is the corresponding reduction peak of Fe^{II}-oxides in the cathodic scan. Peak II ($E \approx -0.75\ V_{SCE}$) is generally assigned to the formation of magnetite (Fe_3O_4) from the Fe^{II} oxidation, corresponding to Eqs. (5) and (6) [11]. The parallel cathodic process for Fe_3O_4 reduction is peak V ($E \approx -0.9\ V_{SCE}$).

$$3\ Fe(OH)_2 + 2OH^- \leftrightarrow Fe_3O_4 + 4\ H_2O + 2\ e^- \quad (5)$$

$$3\ FeO + 2OH^- \leftrightarrow Fe_3O_4 + H_2O + 2\ e^- \quad (6)$$

At potentials more anodic than -0.6 V vs. SCE, the Fe^{III} oxide species are considered to be formed within the passivation potential domain [11], in which the current is maintained at low values until reaching the oxygen evolution potential (peak III; $E \approx 0.55\ V_{SCE}$). Peak IV in the cathodic scan is attributed to the reduction of Fe^{III} oxide species.

For both specimens (A1 and B1), the maximum current associated with peak II increased with cycling, which suggests magnetite formation and accumulation in the passive layer (Fig. 11). By comparing the cyclic voltammograms for samples A1 and B1, a cathodic shift in peak II for sample B1 (pH 13.9) was recorded with respect to the same peak in sample A1 (pH 12.8). This generally reflects an enhanced oxidation

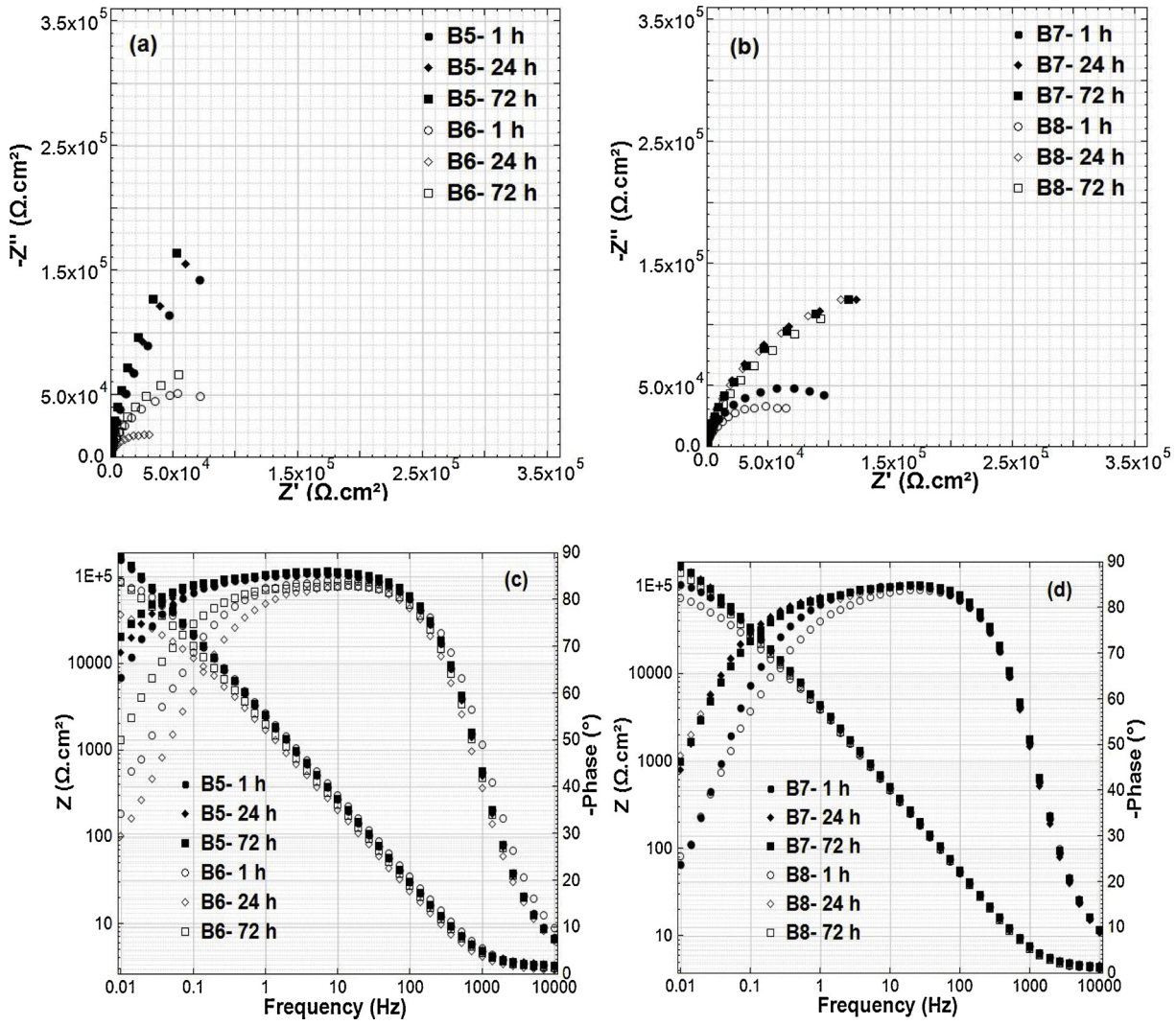

Fig. 9. Overlay of Nyquist (a,b) and Bode (c,d) diagrams of carbon steel after 1, 24 and 72 h of immersion in chlorid-containing B5-B6 and B7-B8 solutions.

reaction with the predominance of Fe^{2+} species, following the reaction mechanisms in Eq. (3). Next, enhanced oxidation and product layer formation after treatment and prior to the CV tests, would result in a steel surface that was covered with a larger amount of corrosion products. This is also evident from the larger reduction currents, as observed from scanning the B1 specimens, if the currents associated with peaks IV and V are compared with those for the A1 specimens. Therefore, the cathodic shift of peak II for the B1 specimens, together with the higher peak current density, can be explained by greater activity (transformation of Fe^0 to Fe^{2+}) and possibly higher Fe^{2+} content, resulting in a higher Fe^{2+}/Fe^{3+} ratio [10,15,49] compared to A1 specimens.

The above results and considerations explain the reason for the increased corrosion current density values (i_{corr}) for B1 specimens, compared to A1 specimens (Fig. 2) and for the cathodic shift in E_{corr} for the same immersion time (Fig. 2). Furthermore, the reduction process with cycling in B1 is apparently different from that in A1, as shown in the responses for the reduction peaks IV and V in Fig. 11a,b. In the case of A1 specimens, by increasing the number of cycles, there was a clear increase in the currents associated with the cathodic peaks, if these are compared to the first cycles. This behavior was reversed in the B1 specimens, where the maximum cathodic currents were measured for the first scan (cycle 1). On increasing the number of CV cycles, a relatively lower cathodic current was measured for the B1 specimens. In addition, the cathodic peaks shifted to more cathodic potentials after the 5th and 10th cycles.

3.4.2. Comparison of the 10th cycles for control specimens A and B

Fig. 12 depicts an overlay of the 10th cycles for carbon steel immersed in chloride-free solutions with pH 12.8 (A1, A2, A3, and A4) and solutions with pH 13.9 (B1, B2, B3, and B4). The passive film formation for A2 specimens (in the presence of 0.016% NMCS) appeared similar to the pattern already observed for A1 specimens (Figs. 11 and 12a). Nevertheless, some differences in peaks I, II, V, and VI were observed. A slight increase in the current density, associated with peak II in A2, accounted for a possible enhancement in the oxidation process in the presence of NMCS when compared to control A1 specimens. Furthermore, the cathodic reduction of Fe^{2+} oxides in peak VI resulted in a lower reduction current and a pronounced broadening of peaks IV and V (Fig. 12). All these features are obviously due to the presence of NMCS alone and their catalytic properties towards the reduction of iron oxides. These changes in the positions of reduction peaks, and the behavior and level of cathodic currents were not observed in the case of specimens A6 and A7, where F127 was present in the medium.

In 0.1 M NaOH solutions with only F127 (A3 specimens), an increase in the current at peak I was recorded, accompanied by a clear decrease in the current at peak II, together with a shift to more cathodic potential. This can be explained by the formation of a less stable passive film, formed in the presence of F127, or in fact, limitations obstructing

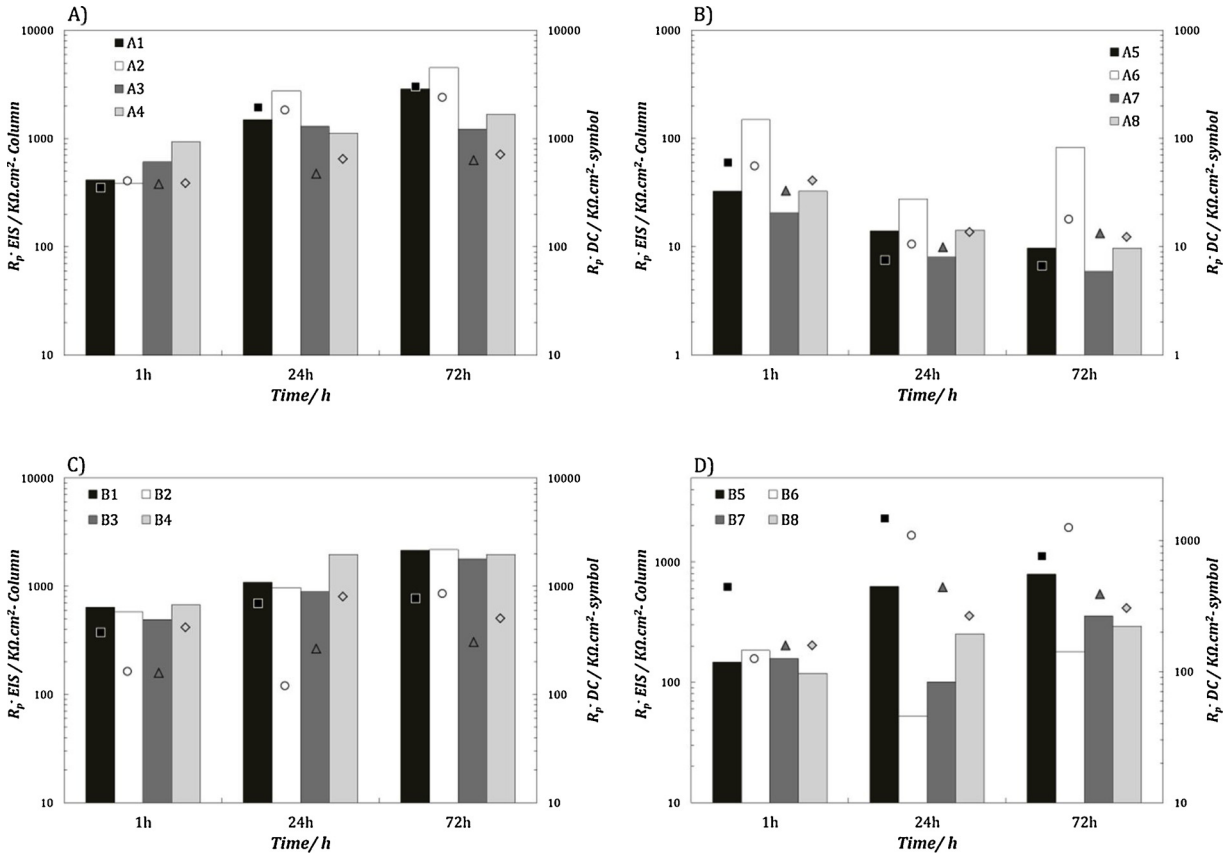

Fig. 10. Comparision of polarization resistance R_p, measured by DC and AC methods (LPR and EIS): A,B) 0.1 M NaOH solutions and (C,D) 0.9 M NaOH solutions after 1, 24 and 72 h of immersion in chlorid-free and chlorid-contaminated solutions.

passive film formation. In addition, the reduction peaks corresponding to magnetite (Fe^{2+} to Fe^{3+} transition) were diminished in the case of A3 specimens (Fig. 12a). Therefore, as was also discussed with regard to corrosion potential and corrosion current evolution with time (Fig. 2a), the presence of F127 impeded the passive film growth and consequently altered the kinetics of the reduction reactions during the cathodic scans. This variation on the steel surface in the presence of F127 also affected the oxygen evolution reaction (peak III), which was shifted to more anodic potentials, another result of an F127-blocked surface.

The CV scans for the A4 specimens were similar to those for A2 specimens in the cathodic scans, except for the lack of broadening and lower current densities at the reduction peaks IV to VI. Additionally, the lowest anodic currents in the forward (anodic) scan were observed for specimen A4 (peaks I and II). This was in contradiction with the highest corrosion current density values being recorded for A4, however, which supports the previously discussed competition between F127 and NMCS, when both are present in the medium. In other words, stable passive film formation was obstructed due to the F127-blocked surface, even though there was NMCS-induced enhancement of the cathodic reaction. This resulted in higher corrosion current densities (Fig. 2a), despite the lower anodic currents with external polarization during CV.

In 0.9 M NaOH solutions (Fig. 12b), the presence of 0.016% NMCS had a quite different effect. For instance, the presence of 0.016% NMCS, in the case of specimen B2, promoted a significant decrease in the current density at peak II (magnetite formation), as well as at the reduction peaks IV, V, and VI. This adverse effect of the NMCS on the steel surface performance (compared to the A specimens) was obviously related to the effect of the higher pH (13.9 in this case) on the NMCS properties, an effect also observed during the zeta potential tests (Table 2). Similarly, for specimens B3 and B4 (steel treated in the presence of F127 and NMCS + F127, respectively) the effect of additives in the testing medium resulted in a different response to the analogous cases in solutions with lower pH, i.e. the cases of A3 and A4.

The presence of F127 (specimen B3) induced pronounced increases in peak I and peak II, together with a cathodic shift of peak II. These features indicated an increase in the Fe^{2+}/Fe^{3+} ratio in the passive film for the B3 specimens and reduced corrosion resistance, compared to specimens B1, B2, and B4. This response is also in line with the highest current density being observed for specimen B3, compared to all the other B specimens in this group (Fig. 2b). Specimens B2 and B4 presented the lowest anodic and cathodic current densities in the forward and reverse scans, accounting for the positive effect of the NMCS, which was especially pronounced in the case of B2, where only NMCS were present in the solution.

3.4.3. CV response in 0.9 M NaOH in the presence of 3.5% NaCl

As previously recorded via LPR and EIS, the CV response of steel in 0.9 M NaOH solutions in the presence of chlorides (specimens B6 to B8) clearly revealed behavior similar to that of the control, chloride-free cases (Fig. 13). The main difference from the analogous control B samples is in the pronounced peak I, assigned to the Fe^0 to Fe^{2+} transition in accordance with Eqs. (3) and (4). This is logical and as expected, since the corrosion process was inevitably initiated due to the presence of chloride ions, but it did not propagate further and was not sustained. This result is in accordance with the initially higher corrosion current density (Fig. 3b), which was further reduced to below the threshold for the active/passive state.

Another observable difference is in the effects of the added F127 and NMCS in the chloride-containing 0.9 M NaOH. Specimen B5, steel treated in an additive-free medium, presented a shift in the voltammogram in the anodic direction and higher current density levels at the characteristic peaks in both the anodic and the cathodic scans. For

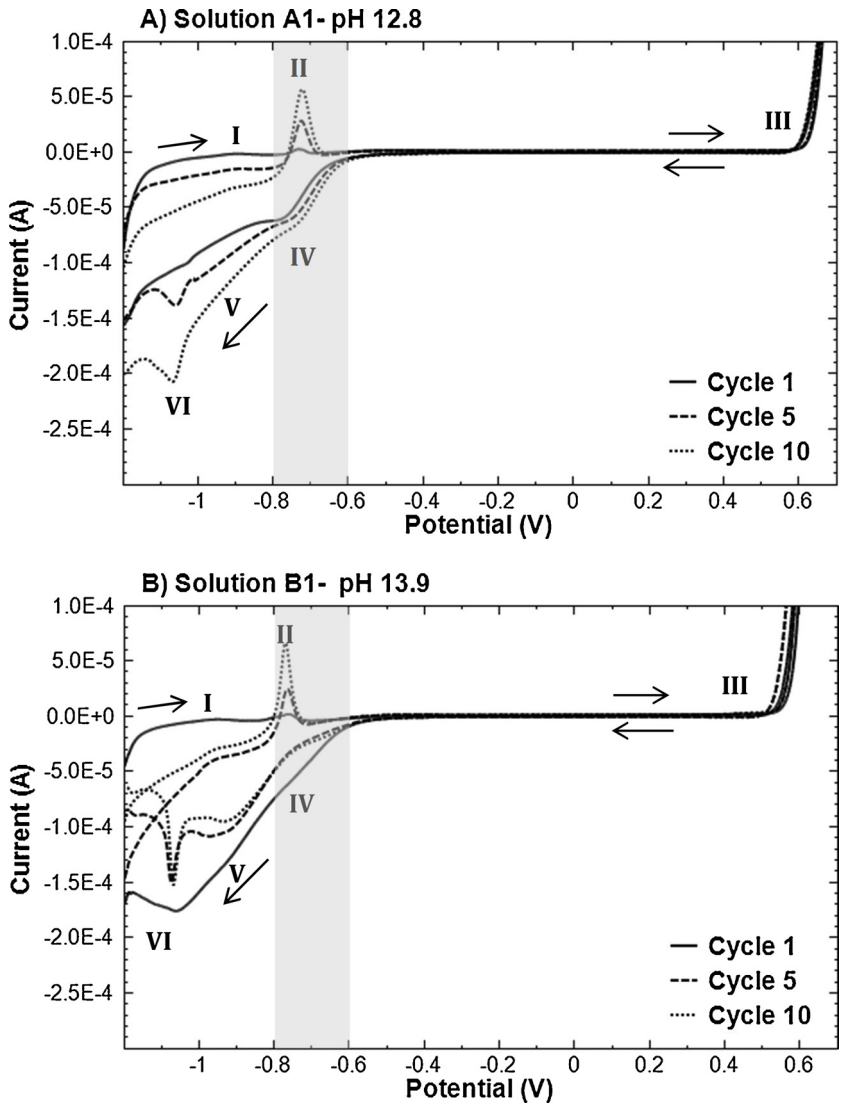

Fig. 11. Cyclic voltammograms of carbon steel samples for selected cycles after 72 h of immersion in chloride-free (a) 0.1 M NaOH solution (A1) and (b) 0.9 M NaOH (B1).

specimens B6, B7, and B8, the current associated with the magnetite formation peaks was reduced, and the peak potential shifted to more negative values (Fig. 13). This shift in the peak potential can be explained by a possible increase in the Fe^{2+}/Fe^{3+} ratio [10,15] in the passive film formed in the presence of NMCS and 3.5% Cl^-, which is similar to the previously recorded behavior in chloride-free solutions (specimens B1–B4, Fig. 12b). The relatively lower corrosion activity of specimens B6 to B8 in this medium is attributed to the competition involving OH^- vs. Cl^- ion activity in the medium, as altered by the presence of F127 and/or NMCS. These mechanisms have already been discussed in the previous sections and are supported by the discussion on the relevant mechanisms in passive layer formation or corrosion activity.

3.4.4. Passive layer formation or dissolution in the presence of additives – relevant mechanisms

Fundamentally, at the metal/film interface, iron ions enter the oxide as Fe^{2+}. The mechanism for this process was proposed elsewhere and is detailed in the following equations [50,51];

$$Fe + V_{Fe}^{3'} \rightleftharpoons Fe'_{Fe} + 2e' \quad (7)$$

$$Fe \rightleftharpoons Fe'_{Fe} + \left(\frac{x}{2}\right)V_{\dot{O}} + 2e' \quad (8)$$

$$Fe'_{Fe} \rightleftharpoons Fe^{x}_{Fe} + 1e' \quad (9)$$

where, Fe'_{Fe} corresponds to the Fe^{2+} ion in the inner layer lattice, Fe^{x}_{Fe} refers to the Fe^{3+} ion, $V_{Fe}^{3'}$ is an Fe^{3+} vacancy, and $V_{\dot{O}}$ represents an oxygen vacancy.

At the barrier layer/solution interface, the passive film growth and dissolution were expected to be simultaneously taking place as follows:

$$V_{\dot{O}} + OH^-_{ad} \rightleftharpoons O^{x}_{O} + H^+ \quad (10)$$

$$Fe^{x}_{Fe} \rightleftharpoons Fe^{3+}_{aq} + V_{Fe}^{3'} \quad (11)$$

In this process, Fe^{3+} vacancies ($V_{Fe}^{3'}$) are generated at the oxide/solution interface and are consumed at the metal/oxide interface.

It has been reported that the presence of carbon-based materials in the vicinity of the passive film (or steel/solution nterface) could alter the semiconductor properties, because of their tendency to accept the excess electrons from the oxygen vacancies [51]. Consequently, in the presence of NMCS (specimens A2, B2), the passive film was expected to have a higher donor concentration than in their absence (specimens A1 and B1). The higher the carrier density, the greater will be the passive film conductivity [52–54]. Consequently, this increase in the

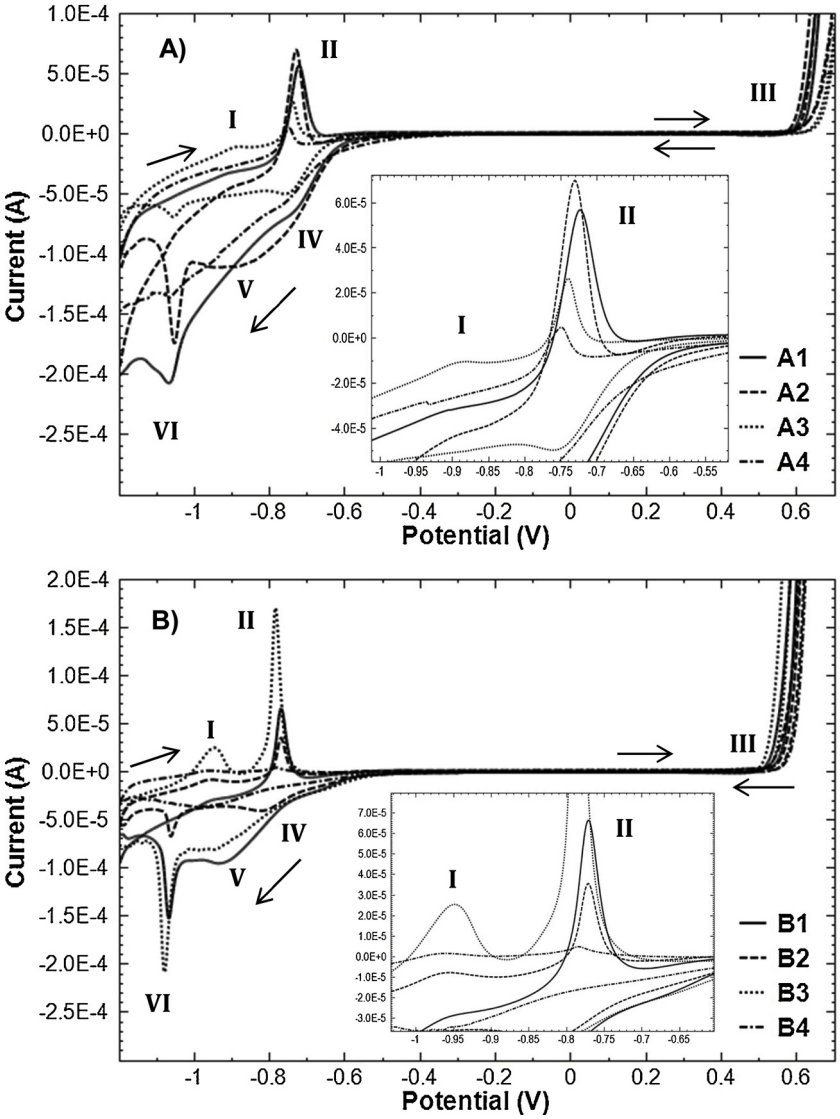

Fig. 12. Comparison of the 10th cycles of carbon steel samples after 72 h of immersion in chloride-free (a) 0.1 M NaOH solution (A1, A2, A3, and A4) and (b) 0.9 M NaOH (B1, B2, B3 and B4). The insets are enlargements of the peaks I and II regions.

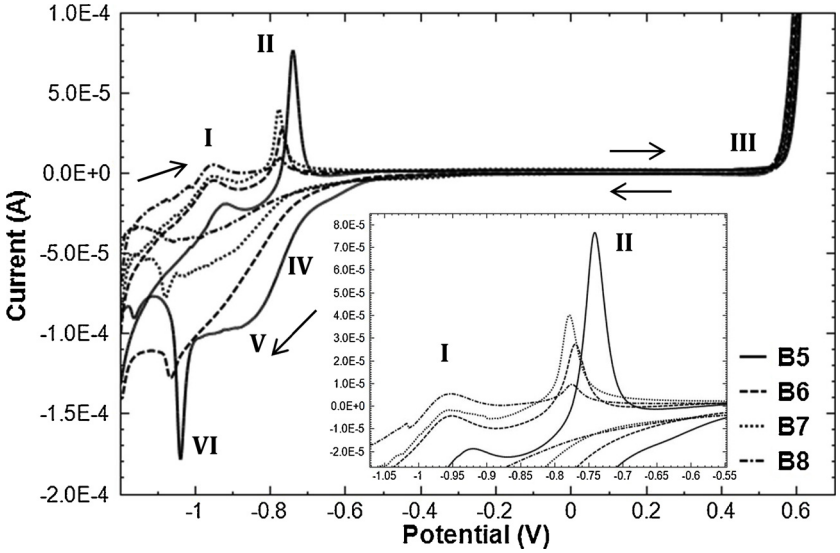

Fig. 13. Comparison of the CV curves of the 10th cycle for carbon steel samples after 72 h of immersion in 0.9 M NaOH solution (samples B5, B6, B7, and B8) in the presence of 3.5% Cl^-. The inset is an enlargement of the peaks I and II ranges.

conductivity leads to higher values of corrosion current density than in the additive-free case, i.e., is in agreement with the i_{corr} values displayed in Fig. 2. Furthermore, this can explain the decrease in the current density associated with the anodic and the cathodic peaks, as appears in the cyclic voltammograms in the presence of NMCS that are shown in Fig. 12. On the one hand, for instance in the case of A4 specimens, the NMCS were expected to be preferentially attracted to surface oxygen vacancies, appearing as sites of high positive charge. In this case, Eq. (10) was expected to be hindered, which can explain the decrease in peak current in the case of A4 specimens (Fig. 12a). This fact was confirmed by the derived corrosion potentials and currents, where in the case of A4 solutions, the treated steel samples showed higher corrosion activity compared to the A1 control specimens (Fig. 12a).

On the other hand, with increasing pH of the environment, e.g. for the case of B4 specimens, the NMCS would affect the mobility of the cation vacancies ($V_{Fe}^{3'}$) (highly negatively charged sites) in the passive film. This can cause retardation in the reactions following Eqs. (7) and (9), which can explain the reason for the observed changes in the anodic and cathodic peaks for the treated steel in the B4 solution (Fig. 12b) and is in line with the cathodic potentials and relatively large corrosion currents, as observed for B4 specimens (Fig. 2b).

In the presence of chloride, the chloride ions could be absorbed into a surface oxygen vacancy, but this must be done at the expense of considerable dehydration [13]. In the presence of NMCS, however, the absorption of chloride on the steel surface meets interference from NMCS. This interference between the chloride absorption, leading to passive film breakdown, and the NMCS on the steel interface is the reason for the increased overall corrosion resistance in B samples in chloride-containing medium, especially in the case of the B6 and B8 specimens, in the presence of NMCS + F127. This performance was not monitored in the case of the B7 solutions with only F127.

4. Conclusions

The characterization of the NMCS particles in alkaline model solutions indicated that they adopt negative charge in NaOH solutions with pH ≤ 12. Increasing the pH of the solutions from 10 to 12 lowers the negative charge. In solutions with pH > 12, i.e. at pH 13 and pH 14, positive zeta potentials for the NMCS particles were recorded.

In chloride-free alkaline solutions with pH 12.8, the presence of 0.016% NMCS induced blocking of the cathodic sites and limitation of the reduction process explains the anodic shift in the corrosion potential of steel samples treated in NMCS or NMCS + F127 solutions. This shift in the potential after 24 and 72 h was not observed in the case of the only F127 in the medium. In 0.9 M NaOH solutions, the NMCS improved the performance of the adsorbed layer on the steel surface, and low corrosion currents were measured. Moreover, in 0.9 M NaOH solutions (pH 13.9), at a given immersion time, a more conductive passive film with a higher Fe^{2+}/Fe^{3+} ratio was developed compared to the layer developed in 0.1 M NaOH.

In the presence of 10% non-ionic Pluronic F127 or 0.016% NMCS dispersed by 10% F127, a less oxidized passive layer was expected due to the blocking of the surface by an adsorbed layer of F127. This resulted in a retardation of the passive film formation. This surface blocking also caused a shift in the oxygen evolution peak to more anodic values. In 0.1 M NaOH solutions with 3.5% Cl^-, relatively lower i_{corr} values were measured in the presence of NMCS and/or 10% F127 than in additive-free solutions, suggesting possible trapping of chloride ions in the porous, positively charged NMCS (undispersed) that could limit the available chloride for corrosion propagation. In the presence of 3.5% Cl in 0.9 M NaOH, the addition of 0.016% NMCS induced a reduction in the magnetite peak formation, and the peak potential shifted to a more anodic value. Furthermore, the oxidation peak of the Fe/Fe^{2+} current increased in the presence of 0.016% NMCS and/or 10% F127.

Declaration of Competing Interest

None.

Acknowledgements

This work is part of a larger research framework on the application of nanomaterials for self-healing of corrosion damage, developed and executed in Delft University of Technology (TU Delft), Faculty CiTG, M &E, supported by Agentschap NL (projects SHM01041 and SHM08743) and performed during the postdoctoral fellowship of Dr. Hitham Mahmoud Amin at TU Delft. The author would like to thank Dr. Koleva (CiTG, TU Delft, Netherlands), Dr. Liu, Prof. Yamauchi (NIMS, Japan) for the supervision of the current work and supplying the NMCs particles.

Appendix A. Supplementary data

Supplementary material related to this article can be found, in the online version, at doi:https://doi.org/10.1016/j.mtcomm.2019.100677.

References

[1] J. Williamson, O.B. Isgor, The effect of simulated concrete pore solution composition and chlorides on the electronic properties of passive film on carbon steel rebar, Corros. Sci. 106 (2016) 82–95.
[2] D.A. Koleva, N. Boshkov, K. van Breugel, J.H.W. de Wit, Steel corrosion resistance in model solutions containing waste materials, Electrochim. Acta 58 (2011) 628–646.
[3] N. Etteyeb, X.R. Nóvoa, Inhibition effect of some trees cultivated in arid regions against the corrosion of steel reinforcement in alkaline chloride solutions, Corros. Sci. 112 (2016) 471–482.
[4] M. Liu, X. Cheng, X. Li, C. Zhou, H. Tan, Effect of carbonation on the electrochemical behavior of corrosion resistance low alloy steel rebars in cement extract solutions, Constr. Build. Mater. 130 (2017) 193–201.
[5] G.S. Duffó, S.B. Farina, Electrochemical behaviour of steel in mortar and in simulated pore solution: analogies and differences, Cem. Concr. Res. 88 (2016) 211–216.
[6] C. Andrade, M. Keddam, X.R. Nóvoa, M.C. Perez, C.M. Rangel, H. Takenouti, Electrochemical behaviour of steel rebars in concrete: influence of environmental factors and cement chemistry, Electrochim. Acta 46 (2001) 3905–3912.
[7] U. Angst, B. Elsener, C.K. Larsen, O. Vennesland, Critical chloride content in reinforced concrete—a review, Cem. Concr. Res. 39 (2009) 1122–1138.
[8] S. Goni, C. Andrade, Synthetic concrete pore solution chemistry and rebar corrosion rate in the presence of chlorides, Cem. Concr. Res. 20 (1990) 525–539.
[9] S. Haupt, H.H. Strehblow, Combined electrochemical and surface analytical investigation of the formation of passive layers, Corros. Sci. 29 (1989) 163–182.
[10] C. Alonso, C. Andrade, M. Izquierdo, X.R. Nóvoa, M.C. Perez, Effect of protective oxide scales in the macrogalvanic behaviour of concrete reinforcements, Corros. Sci. 40 (1998) 1379–1389.
[11] S. Joiret, M. Keddam, X.R. Novoa, M.C. Perez, C. Rangel, H. Takenouti, Use of EIS, ring-disk electrode, EQCM and Raman spectroscopy to study the film of oxides formed on iron in 1 M NaOH, Cement Concrete Comp. 24 (2002) 7–15.
[12] H.B. Gunay, P. Ghods, O.B. Isgor, G.J. Carpener, X. Wu, Characterization of atomic structure of oxide films on carbon steel in simulated concrete pore solutions using EELS, Appl. Surf. Sci. 274 (2013) 195–202.
[13] D.D. Macdonald, The point defect model for the passive state, J. Electrochem. Soc. 139 (1992) 3434–3449.
[14] F. Vicente, J. Gregori, J.J. Garcia-Jareño, D. Gimenez-Romero, Cyclic voltammetric generation and electrochemical quartz crystal microbalanced characterization of passive layer of nickel in a weakly acidic medium, Solid State Electrochem. 9 (2005) 684–690.
[15] L. Freirea, X.R. Nóvoa, M.F. Montemor, M.J. Carmezim, Study of passive films formed on mild steel in alkaline media by the application of anodic potentials, Mater. Chem. Phys. 114 (2009) 962–972.
[16] M. Sanchez, J. Gregori, M.C. Alonso, J.J. Garcia-Jareño, F. Vicente, Anodic growth of passive layers on steel rebars in an alkaline medium simulating the concrete pores, Electrochim. Acta 52 (2006) 47–53.
[17] L.F. Lin, C.Y. Chao, D.D. Macdonald, A point defect model for anodic passive films: II. Chemical breakdown and pit initiation, Electrochem. Soc. 128 (1981) 1194–1198.
[18] E. Sikora, J. Sikora, D.D. Macdonald, A new method for estimating the diffusivities of vacancies in passive films, Electrochim. Acta 41 (1996) 783–789.
[19] P. Marcus, V. Maurice, H.-H. Strehblow, Localized corrosion (pitting): a model of passivity breakdown including the role of the oxide layer nanostructure, Corros. Sci. 50 (2008) 2698–2704.
[20] M.A. Deyab, Effect of carbon nano-tubes on the corrosion resistance of alkyd coating immersed in sodium chloride solution, Prog. Org. Coat. 85 (2015) 146–150.

[21] Z. Pan, L. He, L. Qiu, A.H. Korayem, G. Li, J.W. Zhu, F. Collins, D. Li, W.H. Duan, M.C. Wang, Mechanical properties and microstructure of a graphene oxide-cement composite, Cem. Concr. Compos. 58 (2015) 140–147.
[22] S.M. Park, M.Y. Shon, Effects of multi-walled carbon nano tubes on the corrosion protection of zinc rich epoxy resin coating, Ind. Eng. Chem. 21 (2015) 1258–1264.
[23] F. Collins, J. Lambert, W.H. Duan, The influence of admixtures on the dispersion, workability, and strength of carbon nanotubes-OPC paste mixtures, Cem. Concr. Compos. 34 (2012) 201–207.
[24] F. Sanchez, K. Sobolev, Nanotechnology in concrete—a review, Constr. Build. Mater. 24 (2010) 2060–2071.
[25] N.T. Kirkland, T. Schiller, N. Medhekar, N. Birbilis, Exploring graphene as a corrosion protection barrier, Corros. Sci. 56 (2012) 1–4.
[26] Y. Tong, S. Bohm, M. Song, J. Austin, Carbon based coating on steel with improved electrical conductivity, J. Nanomed. Nanotechnol. 13 (2015) 1041–1047.
[27] C.H. Chang, T.C. Huang, C.W. Peng, T.C. Yeh, H.I. Lu, W.I. Hung, C.J. Weng, T.I. Yang, J.M. Yeh, Novel anticorrosion coating prepared from polyaniline/graphene composites, Carbon 50 (2012) 5044–5051.
[28] E. Sutter, P. Albrecht, F.E. Camino, P. Sutter, Monolayer graphene as ultimate chemical passivation layer for arbitrarily shaped metal surface, Carbon 48 (2010) 4404–4420.
[29] D. Prasai, J.C. Tuberquia, R.R. Harl, G.K. Jennings, K.I. Bolotin, Graphene: corrosion-inhibiting coating, ACS Nano 6 (2012) 1102–1108.
[30] Y.P. Hsieh, M. Hofmann, K.W. Chang, J.G. Jhu, Y.Y. Li, K.Y. Chen, C.C. Yang, W.S. Chang, L.C. Chen, Complete corrosion inhibition through graphene defect passivation, ACS Nano 8 (2014) 443–448.
[31] S. Sreevatsa, A. Banerjee, H. Grebel, Graphene as a permeable ionic barrier, J. Electrochem. Soc. ECS Trans. 19 (2009) 259–264.
[32] R.A. Antunes, M.C.L. Oliveira, G. Ett, V. Ett, Corrosion of metal bipolar plates for PEM fule cells: a review, Int. J. Hydrogen Energy 35 (2010) 3632–3647.
[33] K. Feng, Y. Shen, H. Sun, D. Liu, Q. An, X. Cai, P.K. Chu, Conductive amorphous carbon-coated 316L stainless steel as bipolar plates in polymer electrolyte membrane fuel cells, Int. J. Hydrogen Energy 34 (2009) 6771–6777.
[34] J. Hu, D.A. Koleva, P. Petrov, K. van Breugel, Polymeric vesicles for corrosion control in reinforced mortar: electrochemical behavior, steel surface analysis and buck matrix properties, Corros. Sci. 65 (2012) 414–430.
[35] D.A. Koleva, A.G. Denkova, N. Boshkov, K. van Breguel, Electrochemical performance of steel in cement extract and buck matrix properties of cement paste in the presence of Pluronic 123 micelles, Mater. Sci. 48 (2013) 2490–2503.
[36] J. Hu, D.A. Koleva, J.H.W. de Wit, H. Kolev, K. van Breugel, Corrosion performance of carbon steel in simulated pore solution in the presence of micelles, J. Electrochem. Soc. 158 (2011) C76–C87.
[37] H. Mahmoud, J. Tang, D.A. Koleva, J. Liu, Y. Yamauchi, M. Tade, Concrete Durability vol. 1, Springer, Cham, 2017, pp. 109–137.
[38] J. Tang, J. Liu, C. Li, Y. Li, M.O. Tade, S. Dai, Y. Yamauchi, Synthesis of nitrogen-doped mesoporous carbon spheres with extra-large pores through assembly of diblock copolymer micelles, Angew. Chem. Int. Ed. 53 (2014) 588–593.
[39] T. Yang, J. Liu, R. Zhou, Z. Chen, H. Xu, S.H. Qiao, M. Monterio, N-doped mesoporous carbon shperes as the oxygen reduction catalysts, J. Mater. Chem. A 2 (2014) 18139–18146.
[40] L.L. Zhang, Y. Gu, X.S. Zhao, Advanced porous carbon electrodes for electrochemical capacitor, J. Mater. Chem. A 1 (2013) 9395–9408.
[41] J. Li, Z. Li, J. Tong, C. Xiaa, F. Li, Nitrogen-doped ordered mesoporous carbon sphere with short channel as an efficient metal-free catalyst for oxygen reduction reaction, RSC Adv. 5 (2015) 70010–70016.
[42] M. Stern, A.L. Geary, A theoretical analysis of the shape of polarization resistance curves, J. Electrochem. Soc. 104 (1957) 56–63.
[43] C. Alonso, Corrosion rate monitoring in the laboratory and on-site, Constr. Build. Mater. 10 (1996) 315–328.
[44] E. Zornoza, J. Paya, P. Garces, Chloride-induced corrosion of steel embedded in mortars containing fly ash and spent cracking catalyst, Corros. Sci. 50 (2008) 1567–1575.
[45] K. Gong, F. Du, Z.H. Xia, M. Durstock, L.M. Dai, Nitrogen-doped carbon nanotube Ar-rays with high electrocatalytic activity for oxygen reduction, Science 323 (2009) 760–764.
[46] D.H. Deng, X.L. Pan, L.A. Yu, Y. Cui, Y.P. Jiang, J. Qi, W.X. Li, Q.A. Fu, X.C. Ma, Q.K. Xue, G.Q. Sun, X.H. Bao, Toward N-doped graphene via solvothermal synthesis, Chem. Mater. 23 (2011) 1188–1193.
[47] K. Wan, Z.P. Yu, X.H. Li, M.Y. Liu, G. Yang, J.H. Piao, Z.X. Liang, pH effect on electro-chemistry of nitrogen-doped carbon catalyst for oxygen reduction reaction, Catalysis 5 (2015) 4325–4332.
[48] J. Hu, D.A. Koleva, Y. Ma, E. Schlangen, P. Petrov, K. van Breugel, The influence of admixed micelles on the microstructural properties and global performance of cement-based materials, Cem. Concr. Res. 42 (2012) 1122–1133.
[49] L. Freire, M.J. Carmezima, M.G.S. Ferreiraa, M.F. Montemora, The passive behavior of AISI 316 in alkaline media and the effect of pH: a combined electrochemical and analytical study, Electrochim. Acta 55 (2010) 6174–6181.
[50] R. Basak, R. Bandynopadhyay, Encapsulation of hydrophobic drugs in pluronic F127 micelles: effect of drug hydrophobicity, solution temperature, and pH, Langmuir 29 (2013) 4350–4356.
[51] A. Yazdenbakhsh, Z. Grasley, The theoretical maximum achievable dispersion of nanoinclusions in cement paste, Cem. Concr. Res. 42 (2012) 798–804.
[52] E.B. Castro, Analysis of the impedance response of passive iron, Electrochim. Acta 39 (1994) 2117–2123.
[53] L. Liu, J. Xu, Z.H. Xie, P. Munroe, The roles of passive layers in regulation the electrochemical behavior of Ti_5-Si_3-based nanocomposite films, Mater. Chem. A 1 (2013) 2064–2078.
[54] Y. Xia, F. Cao, W. Liu, L. Chang, H. Zhang, The formation of passive films of carbon steels in borate buffer and their degradation behavior in NaCl solution by SECM, Int. J. Electrochem. Sci. 8 (2013) 3057–3073.